NASA Contractor Report 3721

TAS - A Transonic Aircraft/Store Flow Field Prediction Code

D. S. Thompson

CONTRACT NAS2-11277
DECEMBER 1983

25th Anniversary
1958-1983

NASA

NASA Contractor Report 3721

TAS - A Transonic Aircraft/Store Flow Field Prediction Code

D. S. Thompson
General Dynamics Corporation,
Fort Worth Division
Fort Worth, Texas

Prepared for
Ames Research Center
under Contract NAS2-11277

National Aeronautics
and Space Administration

**Scientific and Technical
Information Branch**

1983

TABLE OF CONTENTS

LIST OF FIGURES

LIST OF FIGURES (Cont'd)

LIST OF TABLES

LIST OF SYMBOLS

Symbol	
A	As a subscript, A denotes the cartesian mesh to be interpolated from
B	As a subscript, B denotes the general mesh containing the point to be interpolated to
C_A	Nondimensional axial force coefficient, positive vector directed aft
C_n	Axial distribution of normal force coefficient
C_N	Nondimensional normal force coefficient, positive vector directed up
C_{NM}	Nondimensional pitching moment coefficient, positive vector directed outboard (nose up)
C_s	Axial distribution of side force coefficient
C_S	Nondimensional side force coefficient, positive vector directed outboard
C_{SM}	Nondimensional yawing moment coefficient, positive vector directed down (nose out)
D	Maximum store diameter
$F_1,F_2,F_3,$ F_4,F_5,F_6	Intermediate interpolation results
F_X	Chordwide variation of fin thickness
L	Store length
M	Freestream Mach number
R_X	Axial variation of body thickness
r	Radial coordinate direction
r_B	Body radius
r_{OB}	Radius of store mesh outer boundary
r_{SFFSS}	Radius of circle centered at x_{ST}, y_{ST}, z_{ST} required to completely enclose the store flow field support surface
x	Chordwise coordinate direction, positive direction aft
x_s	Axial coordinate direction, positive direction aft

LIST OF SYMBOLS (Cont'd)

Symbol	
x_{ST}	X location of store nose
x_{MO}	X location of moment origin (for store)
y	Spanwise coordinate direction, positive direction out the left wing
y_{ST}	Y location of store nose
z	Vertical coordinate direction, positive direction up
z_{ST}	Z location of store nose
α	Angle of attack
β	Angle of yaw
γ	Ratio of specific heats
Δ	Difference operator used in linear interpolation
δ	Difference operator used in linear interpolation
$\mu(x)$	Nonlifting empirical correction
$\nu(\theta,x)$	Lifting empirical correction
θ	Angular coordinate direction
ϕ	Perturbation velocity potential

1. INTRODUCTION

It is well understood and appreciated that weapon certification is an expensive and time consuming process. A myriad of costly wind tunnel and flight tests is required to accomplish this task. Certification of many aircraft/weapon systems is accomplished only after testing several geometric modifications. This is especially true in the transonic flight regime. Transonic interference effects between an aircraft and its component stores can significantly alter separation characteristics and make accurate delivery of an armament to a target exceedingly difficult. In addition, these same interference effects can significantly degrade aircraft performance by reducing the overall aerodynamic efficiency of the configuration. It is paradoxical to note that although the aerodynamic design of a military aircraft requires careful attention to detail to achieve the desired results, little consideration is given to these interference effects during the design cycle. These important interference effects are ignored primarily because no reliable methodology exists to accurately predict the effects of transonic aircraft/store interference. Therefore, methodology is needed which will accurately and efficiently predict the complex aircraft/store interference effects which occur in the transonic flight regime.

The use of computational aerodynamics methodology to predict the aerodynamic characteristics of complex configurations of this type would significantly decrease required wind tunnel and flight testing. In addition, employing computational aerodynamics methodology would give the designer the capability to obviate many of the undesirable effects of transonic aircraft/store interference. This methodology has not been fully exploited due to the absence of sufficiently accurate models for the complex flow fields associated with configurations of this type and also because of the lack of necessary computer capability. However, significant progress is being made in both areas.

Stahara (Reference 1) has reported development of a method to predict three-dimensional transonic flow fields about an aircraft and the load distributions on external stores located in the flow field. The theoretical method, designed for rapid calculations, relies on the classical transonic equivalence rule, which is then extended to account for three-dimensional crossflow effects. One modification replaces the linear two-dimensional crossflow solution with a linear three-dimensional solution obtained by panel

methods. Another correction employs a three-dimensional nonlinear finite difference solution of the small disturbance equations. Results presented for the Nielsen generic store are encouraging. However, no attempt was made to simulate a realistic store with fins.

A method for analyzing store separation characteristics has been developed by Deslandes (Reference 2). The problem is simplified by quasilinearization of the time dependence in the separation dynamics, with a flow angularity technique employed to evaluate first-order interference effects. The method can use theoretically or experimentally determined flow field data for the interference calculations. Good correlation with drop model tests is demonstrated for subsonic Mach number with an angle of attack variation. High transonic Mach number applicability has not been demonstrated in the literature.

Shankar and Malmuth (Reference 3) have developed a method for analyzing aircraft/pylon/store configurations in transonic flow. The method is based on the work done by Ballhaus, Bailey, and Frick (Reference 4) and later refined by Mason, MacKenzie, et al (Reference 5). The modified small disturbance (MSD) equation is solved iteratively using finite difference techniques. The pylon and store are simulated by use of an image point concept. The image point concept avoids excessive storage requirements and lengthened run times due to increased complexity. However, simulation of fins was not demonstrated. The code, with modifications, could be used to simulate horizontal and vertical fins. Simulation of fins with arbitrary angular orientation using this method would be extremely difficult.

Another technique, being developed under the sponsorship of AFWAL, is the Influence Function Method (IFM) of Meyer, Cenko, and Yaros (Reference 6). The IFM technique, although originally developed for supersonic flow, has recently been extended to subsonic and transonic speeds (Reference 7). The basic premise of the IFM technique is that store loads are uniquely dependent on the local angle of attack distribution along the store. Impressive comparisons between IFM results and experimental data were presented in Reference 7. The higher-order panel method code PAN AIR was used to generate the necessary flow field data for the IFM technique.

2. BACKGROUND

In 1979, General Dynamics, in cooperation with NASA ARC, began a long range research program to develop the capability to analyze complex aircraft/store flow fields in the transonic flight regime. The TAS (Transonic Aircraft/Store) code is being develped to form the nucleus of a comprehensive procedure that will predict the transonic carriage and separation characteristics of arbitrary store loadings. The TAS code employs a mesh embedding approach similar to that of Boppe and Stern (Reference 8) in addition to potential flow and small disturbance theories. This method is also an extension of the work of Ballhaus, Bailey, and Frick (Reference 4) and Mason, MacKenzie, et al (Reference 5) for wing/body configurations. The mesh embedding approach eliminates the need for a single continuous computational mesh for the entire configuration. In addition, the mesh embedding approach allows each component of the configuration to be represented by a computational mesh that is suited to its particular surface geometry and length scale. Use of potential flow and small disturbance theories does, of course, place restrictions on the range of application of the code. However, these disadvantages are offset by the simplicity of surface boundary condition application. Linearized flow tangency boundary conditions are applied on a representative mean surface. Remarkably good results have been obtained by codes employing this approach. In the paragraphs that follow, development of the TAS code, up to the subject contract, is summarized. Details of the method are presented in Reference 9.

Initially, the capability was developed to analyze an isolated store in the transonic flight regime. The store geometry was limited to a body of revolution without fins or one set of cruciform fins with arbitrary angular displacement. A cylindrical mesh with angular periodicity was used to discretize the computational domain. Typical results predicted by the isolated store code are compared with experimental data (Reference 10) for the Neilsen generic store in Figure 1. Pressures predicted by the code for a more complex configuration, the GBU-15, are compared with experimental data (Reference 11) in Figures 2 and 3, the body and fin pressure distributions respectively. In Figures 1 and 2, the predicted body pressures show excellent agreement with the experimental data except in the nose region, where small discrepancies occur. These discrepancies, which significantly affect the normal force calculation, are a product of the small disturbance approximation and are discussed in detail in Section 3. The GBU-15 fin pressures (Figure

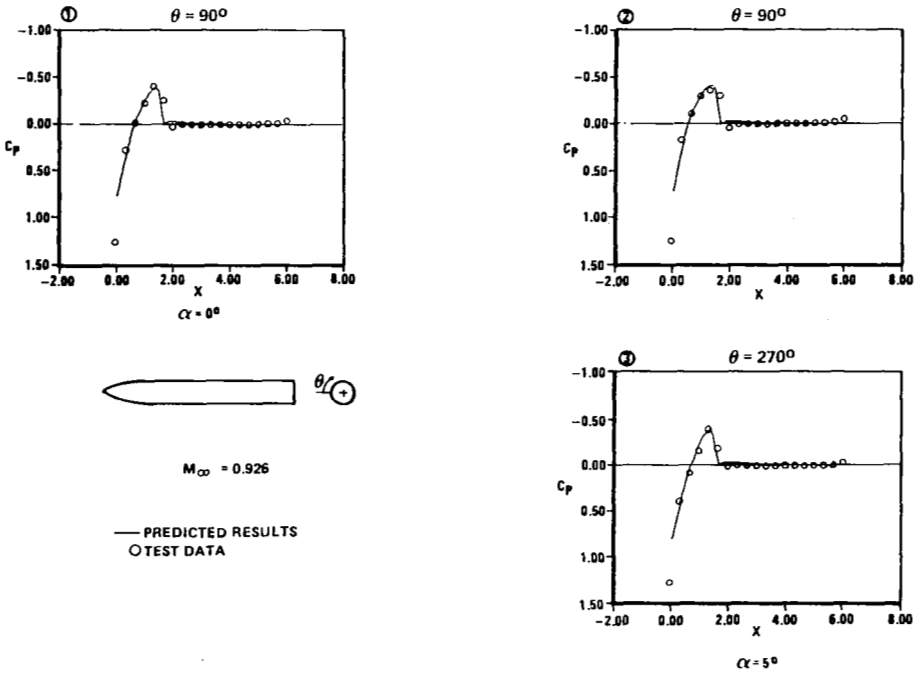

Figure 1 **Predicted Nielsen Store Pressures Show Good Agreement With Test Data (Reference 10)**

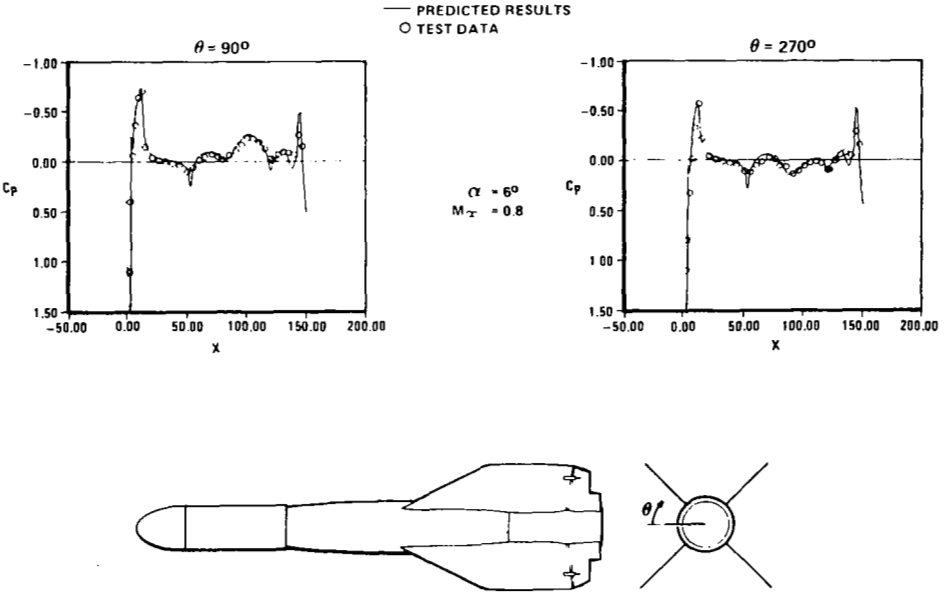

Figure 2 **Predicted GBU-15 Body Pressures Show Good Agreement With Test Data (Reference 11)**

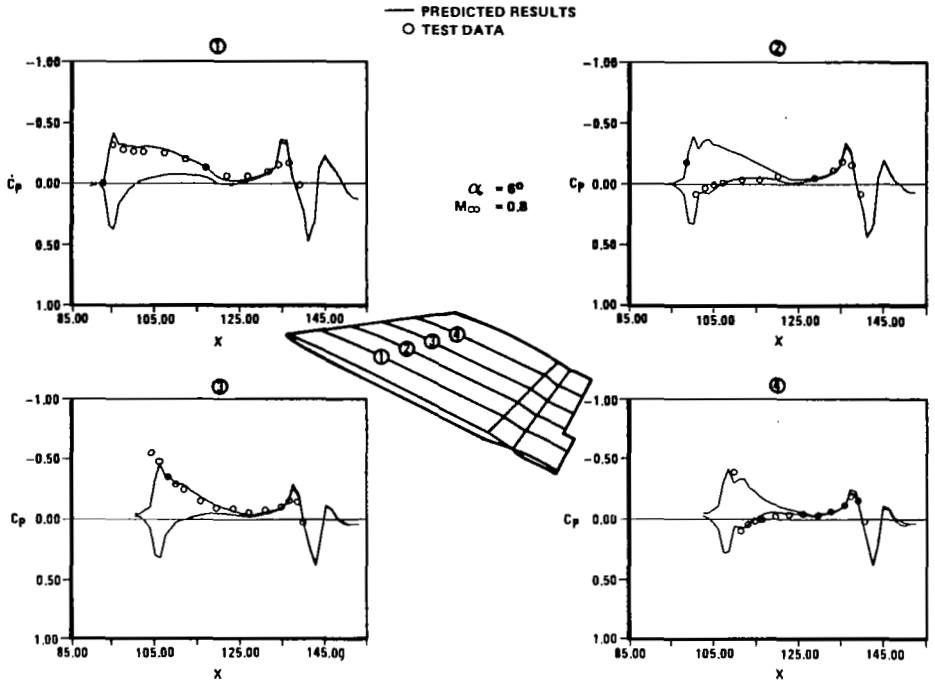

Figure 3 **Predicted GBU-15 Fin Pressures Show Good Agreement With Test Data (Reference 11)**

3) also show good agreement with experimental data except in the region near the leading edge. This discrepancy can be reduced by utilizing a planform oriented coordinate system (Reference 9). In general, good results and favorable convergence characteristics were obtained for the configurations considered.

TAS code development was initiated with NASA Ames funding under Contract NAS2-10779 in 1980. This phase of the program consisted of coupling the isolated store procedure with an existing wing/body code. Due to previous favorable experiences, the Bailey-Ballhaus code (References 4 and 5) was selected. Coupling was accomplished by employing the embedded mesh scheme described below.

The configuration chosen for analysis was an aircraft with a separated store located approximately one wing chord below the aircraft as shown in Figure 4. This configuration was chosen to evaluate the embedded mesh concept and avoid any problems which might be associated with strong aircraft/store interactions. The TAS code utilized three

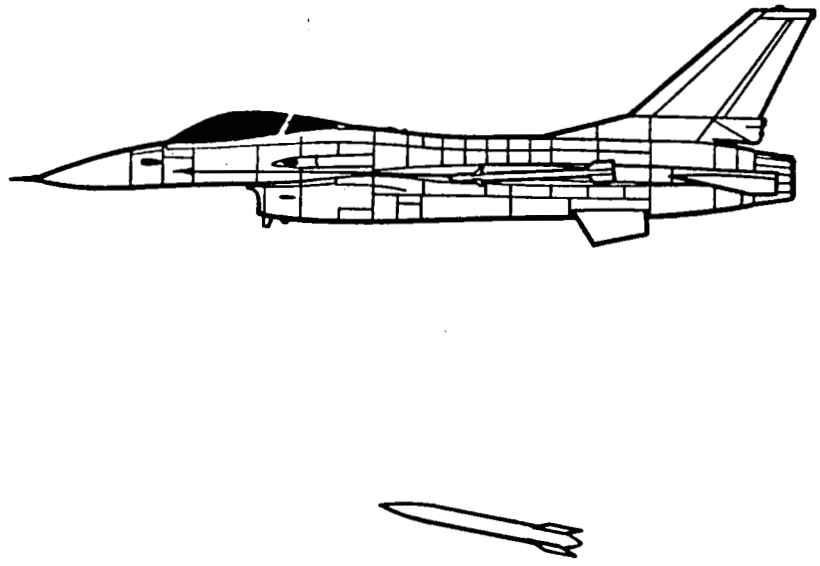

Figure 4 **TAS Code Was Initially Developed for Aircraft/Store Configurations of This Type**

distinct meshes to discretize the computational domain: (1) a planform oriented wing fine mesh, (2) the cylindrical store mesh, and (3) a global Cartesian crude mesh. The embedded mesh system is shown schematically in Figure 5. It is important to note that the store mesh was embedded only in the crude mesh, prohibiting simulation of store carriage. The transonic flow field was obtained by iteratively solving a modified version of the small disturbance potential flow equation on each mesh by successive fine/store/crude mesh relaxations. Dirichlet or Neumann boundary conditions applied at the mesh interfaces were updated during the course of each global iteration. Typical results for the F-16/B-61 configuration shown in Figure 4 are compared with isolated B-61 results in Figure 6. These results are intuitively correct, since aircraft/store interference effects for this configuration should be minimal. No experimental pressure data was available for direct validation of the code. This version of the TAS code served as the starting point for the subject contract.

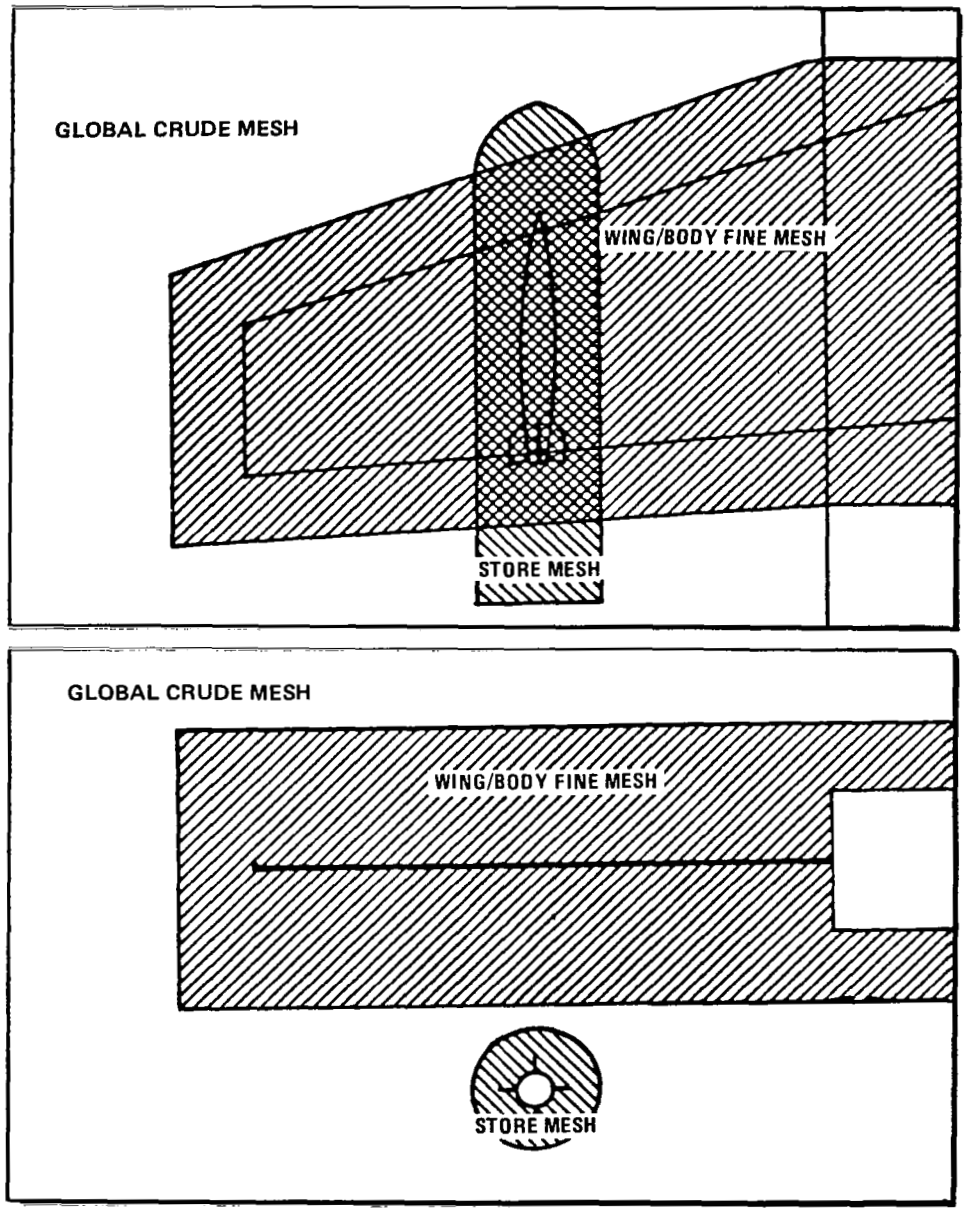

Figure 5 Embedded Mesh Scheme Originally Employed By TAS Code

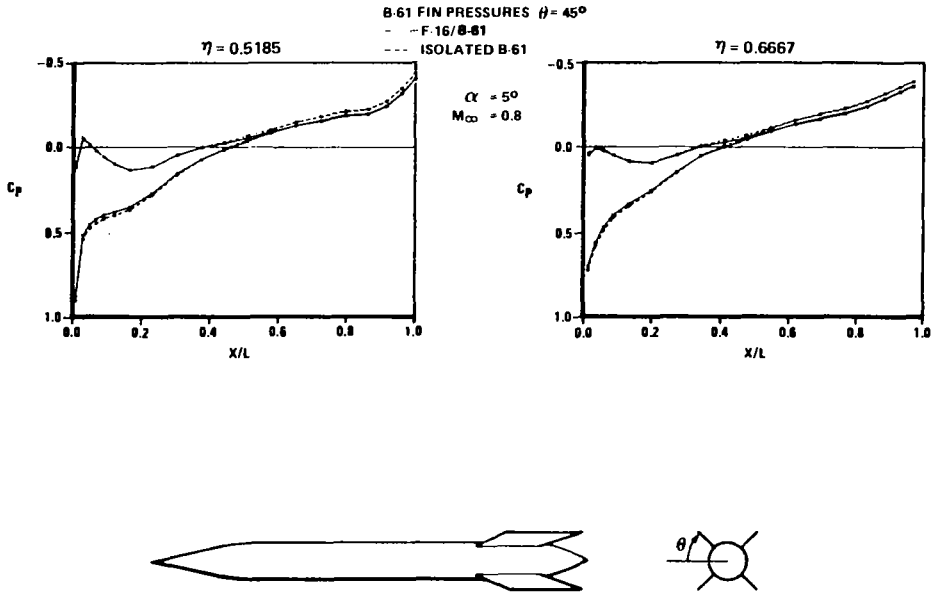

Figure 6 Results Predicted for F-16/B-61 Configuration Are Intuitively Correct

3. ANALYSIS OF STORE IN FINE MESH

The TAS code was modified to allow the store to be located in the wing/body fine mesh. These modifications, performed during the subject contract, permit analysis of the aircraft/store configuration shown in Figure 7. It is important to note that simulation of store carriage is not possible since no provision was made for pylon simulation in the fine and crude meshes. In the following subsections, those aspects of the code pertaining the transonic aircraft/store analysis employed by the TAS code are presented in detail. Details of the wing/body and isolated store analyses are presented in References 5 and 9, respectively.

The two coordinate systems employed by the TAS code are shown in Figure 8. The x, y, z coordinate system is fixed with respect to the aircraft and the x_s, r, θ coordinate system is fixed with respect to the store. Transformation from the store coordinate system to the aircraft coordinate system is given by

$$\begin{aligned} x &= x_s + x_{st} \\ y &= r\cos\theta + y_{st} \\ z &= r\sin\theta + z_{st} \end{aligned} \tag{1}$$

where x_{ST}, y_{ST}, and z_{ST} give the x, y, and z position respectively of the store nose.

The inverse transformation is given by

$$\begin{aligned} x_s &= x - x_{st} \\ r &= ((y - y_{st})^2 + (z - z_{st})^2)^{1/2} \\ \theta &= \tan^{-1}((z - z_{st})/(y - y_{st})) \end{aligned} \tag{2}$$

Similarly, derivatives of the perturbation potential ϕ are transformed as follows:

$$\begin{aligned} \phi_x &= \phi_{xs} \\ \phi_y &= \phi_r\cos\theta - \phi_\theta\sin\theta/r \\ \phi_z &= \phi_r\sin\theta + \phi_\theta\cos\theta/r \end{aligned} \tag{3}$$

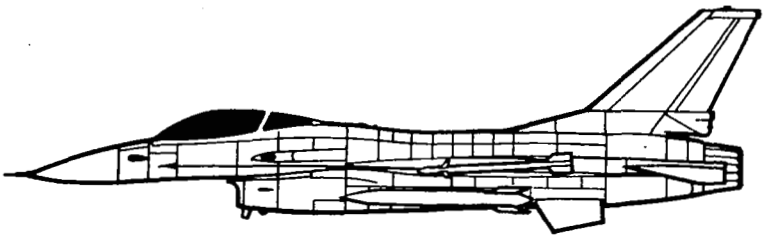

Figure 7 The TAS Code Was Modified to Simulate Configurations of This Type

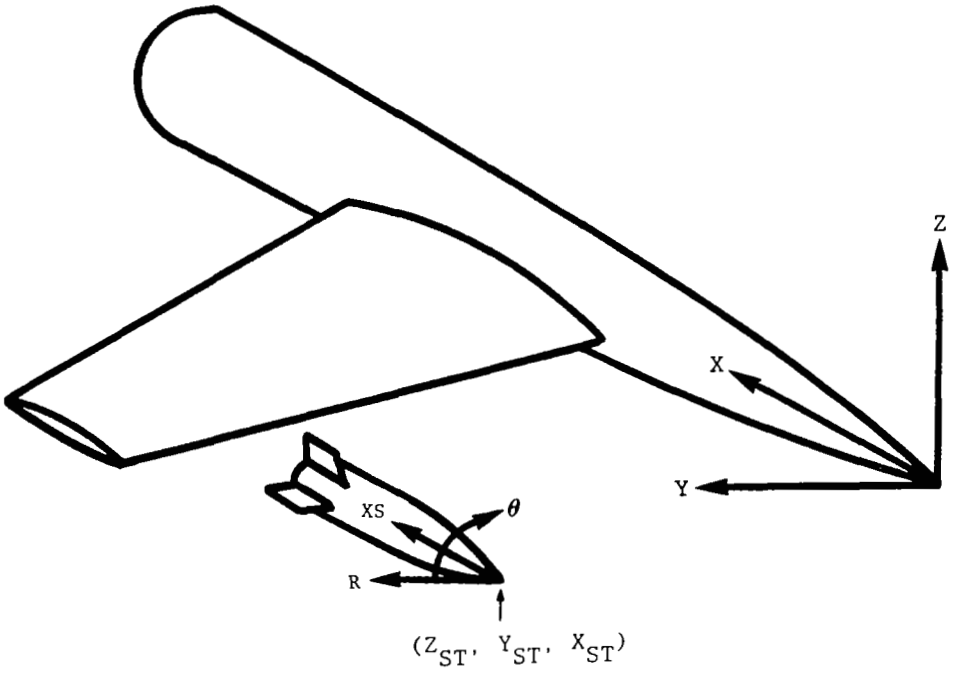

Figure 8 Coordinate Systems Used By The TAS Code

and

$$\phi_{xs} = \phi_x$$

$$\phi_r = \phi_y \cos\theta + \phi_z \sin\theta \qquad (4)$$

$$\phi_\theta / r = -\phi_y \sin\theta + \phi_z \cos\theta$$

where θ on the right hand side of Equation 4 is computed from Equation 2.

3.1 EMBEDDED MESH SCHEME

Discretization of the computational domain used by the TAS code to simulate the aircraft/store configuration shown in Figure 7 was accomplished by a mesh embedding approach. Figure 9 illustrates the embedded mesh system for the aircraft/store configuration under consideration. The two grid system of Reference 5 was employed to discretize the aircraft flow field. A planform oriented fine mesh discretized the region of the flow field near the wing. This fine mesh was embedded in aCartesian global crude mesh that discretized the entire computational domain. A cylindrical store mesh with angular periodicity was embedded in both the fine and crude meshes. As Figure 9 illustrates, it was not necessary for the store mesh outer boundary to be contained completely within a single mesh. Provisions were made in the TAS code to permit a mesh arrangement of this type.

Use of an embedded mesh approach was beneficial for several reasons. Primarily, it eliminated the necessity of having a single continuous mesh system to discretize the entire computational domain. Mesh embedding also allowed use of component adaptive meshes or meshes which better represent the geometry of the configuration component they surround. In the TAS code, the cylindrical store mesh was a component adaptive mesh used to improve simulation of the store geometry. In addition, the flow field governing equations can be formulated independently in each mesh system allowing more accurate (more complex) treatment of localized regions of the flow field. This feature was not exploited during development of the TAS code. In a separate effort, General Dynamics has initiated development of a time accurate transonic aircraft/store flow field prediction code utilizing dynamic mesh embedding coupled with a zonal approach.

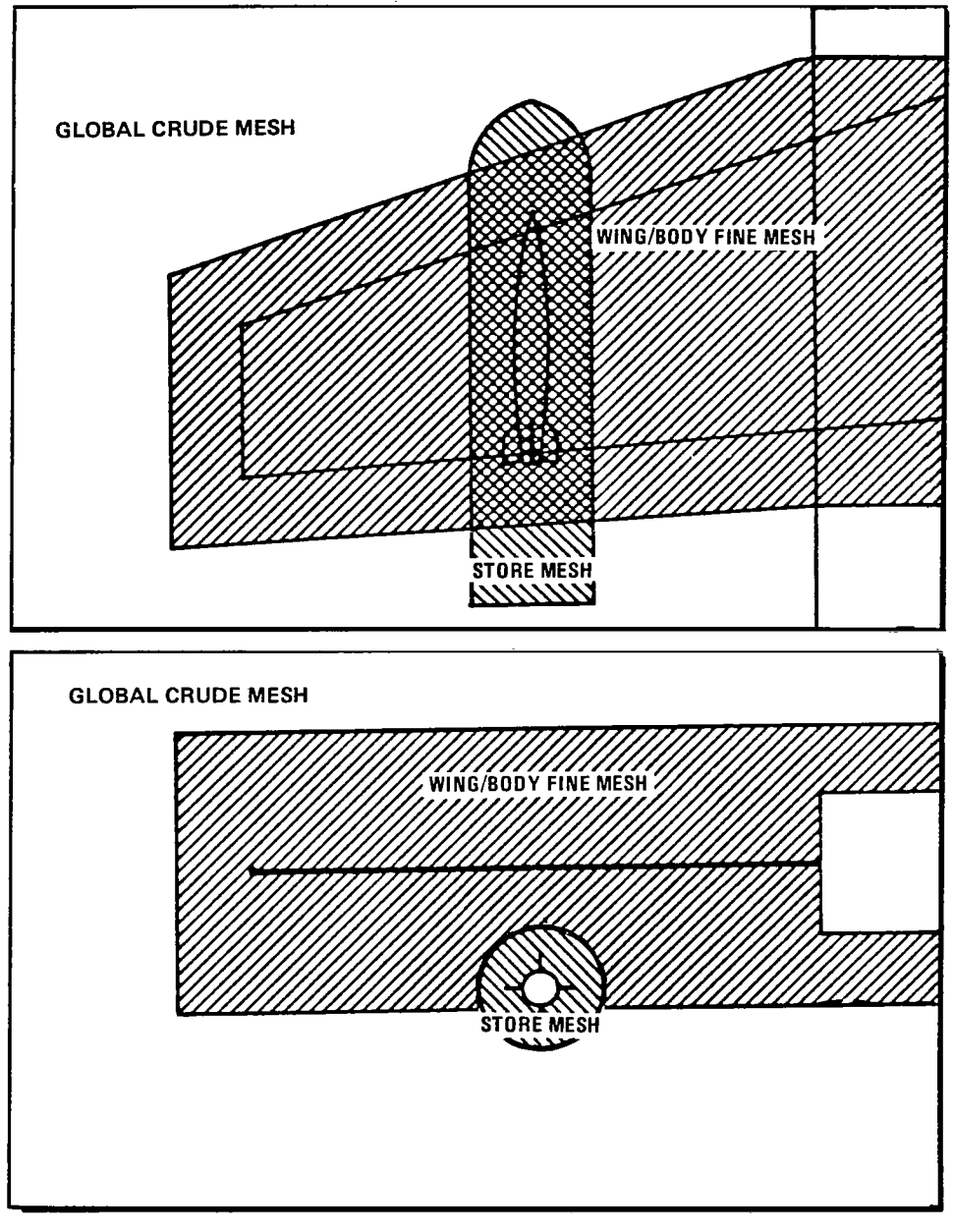

Figure 9 Embedded Mesh Scheme Employed For Arbitrarily Located Store

The distinctive feature of the method was that an additional mesh was used exclusively for the store. This lengthened TAS code run times and increased computer storage requirements. However, the advantages of using a cylindrical mesh with angular periodicity, in terms of configuration simulation, more than offset these disadvantages. Most significantly, a cylindrical mesh eliminated the need for interpolation at the fin mean surfaces for noncruciform fin orientations. Angular coordinate lines were concentrated near fin positions to allow resolution of gradients normal to the fin surface. In addition, the version of the transonic small disturbance potential flow equation that was solved contained additional higher-order terms for better resolution of swept shockwaves on the wing. In cyclindrical coordinates, these extra terms described flow on a plane defined by a constant angular coordinate. Only one flow equation was necessary for fins with arbitrary angular orientation. This can be contrasted to the work of Boppe and Stern (Reference 8), where a cartesian mesh was used and different flow equations are used for wing (x-y plane) and winglet (x-z plane) surfaces.

As in any mesh embedding approach, information was transmitted between meshes by applying interpolated boundary conditions at the various mesh interfaces. Details of these interpolations are presented in Section 3.4. In the basic wing/body code, information transmittal between the fine and crude meshes occurred at two locations: (1) the outer boundary of the fine mesh and (2) the surface of the wing/body located within the fine mesh. Dirchlet (potential) boundary conditions interpolated from results of the crude mesh relaxation were applied on the outer boundary of the fine mesh. This procedure transmitted the effects of the farfield boundary conditions to the fine mesh. Dirichlet boundary conditions interpolated from the results of the fine mesh relaxation were applied on the crude mesh surfaces representing the wing/body that were located within the fine mesh. Neumann boundary conditions were applied on the portion of the body located outside the fine mesh.

Information transmittal between the store mesh and the fine and crude meshes was accomplished in an analogous manner. The primary difference between the procedures was that results of a store mesh relaxation cycle were transmitted to the fine and crude meshes through a prism of rectangular cross-section denoted as the store flow field support surface (SFFSS). Figure 10 illustrates the mesh configuration with the SFFSS included for clarity. The TAS code actually defined two SFFSS, one each for the fine and crude meshes. The SFFSS in each mesh did not necessarily occupy the same physical space. Each SFFSS was initiated upstream of the store and extended to the downstream boundary of its respective computational domain completely enclosing the store and the associated system of fin vortex sheets. Since each SFFSS was essentially a boundary, no

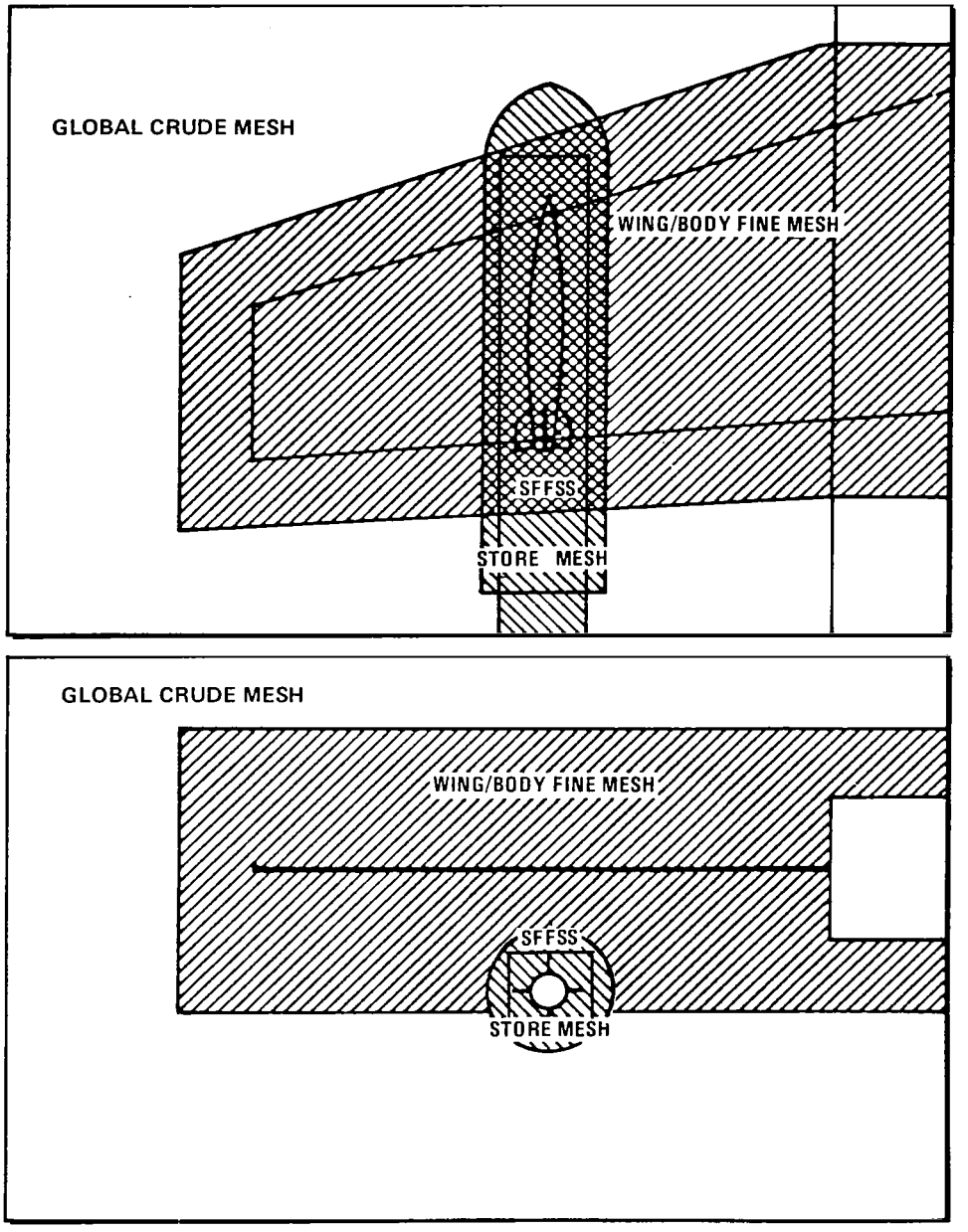

Figure 10 Embedded Mesh Scheme With SFFSS Shown

relaxation was required on the interior of each SFFSS. In essence, the store geometry was removed from the fine and crude mesh relaxation process. This allowed fins of arbitrary angular orientation to be simulated without excessive complication of the fine and crude mesh solution algorithms.

The outer boundary of the store mesh, in general, was not completely contained within one mesh as illustrated in Figures 9 and 10. Boundary conditions applied on the store mesh outer boundary were obtained by interpolation from the appropriate surrounding mesh. The strategy employed by the TAS code was to first interpolate the store mesh outer boundary conditions exclusively from the crude mesh. Then interpolate the boundary conditions from the fine mesh for the store mesh outer boundary points that are located within the fine mesh. This procedure was utilized primarily because of simplicity. No complex logic was required to implement this approach.

One potential difficulty associated with mesh embedding was mesh overlap. As shown in Figure 10, there was a region of the computational domain that was common to both the store and the fine meshes. The numerical solution in this region was computed independently on each mesh. The common regions were coupled only through the boundary conditions applied on the store mesh outer boundary and the SFFSS. Thompson (Reference 9) and Atta (Reference 12) have previously shown that the degree of mesh overlap has a significant influence on the convergence characteristics of an iterative procedure employing a mesh embedding approach. In general, increasing the size of the overlap region improved convergence of the iteration. However, this was inefficient since mesh points are wasted as the overlap region increases in size. Numerical experiments (Reference 12) indicated that $0.75 \leq r_{SFFSS}/r_{OB} \leq 0.85$ was nearly optimum.

3.2 GOVERNING EQUATIONS

The modified small disturbance (MSD) potential equation for transonic flow written in terms of the disturbance velocity potential ϕ is given in conservation form by

$$[(1 - M_\infty^2)\,\phi_x - ((\gamma + 1)/2)\,M_\infty^{1.75}\phi_x^2 + \underline{(1 - M_\infty^2)\,\phi_y^2}]_x$$

$$- \underline{(1 - ((\gamma - 1)/2)\,M_\infty^2)[\phi_y^2]_x} + [(1 - \underline{(\gamma - 1)M_\infty^2\phi_x})\,\phi_y]_y \qquad (5)$$

$$+ \phi_{zz} = 0$$

in the fine and crude meshes. In Equation 5, M_∞ is the freestream Mach number, γ is the ratio of specific heats, and x, y, and z denote the axial, spanwise, and vertical Cartesian coordinates as defined in Figure 8. The underlined terms are higher-order terms which have been retained to improve resolution of swept shock waves in the x-y plane. Wing and fuselage boundary conditions were discussed at great length in References 4 and 5, so no mention of the procedure is made here except to say that fuselage boundary conditions that have been modified using slender body theory were applied on a prismatic boundary condition support surface (BCSS) in the fine and crude meshes.

In the store mesh, the MSD equation is given in conservation form by

$$[(1 - M_\infty^2)\,\phi_x - ((\gamma + 1)/2)\,M_\infty^{1.75}\phi_x^2 + \underline{(1 - M_\infty^2)\,\phi_r^2}]_x$$

$$- \underline{(1 - ((\gamma - 1)/2)\,M_\infty^2)[\phi_r^2]_x} + (1/r)[(1 - \underline{(\gamma - 1)M_\infty^2\phi_x})\,r\phi_r]_r \qquad (6)$$

$$+ (1/r^2)\phi_{\theta\theta} = 0$$

where x, r, and θ denote the axial (x_S), radial, and angular coordinate directions respectively as defined in Figure 8. The underlined terms are higher-order terms that have been retained to improve resolution of swept shock waves in the x-r plane and are analogous to the underlined terms in Equation 5. The linearized fin and body boundary conditions are given by

$$\phi_\theta/r = F_x - \alpha\cos\theta + \beta\sin\theta \tag{7}$$

and

$$\phi_r = R_x - \alpha\mathrm{SIN}\theta - \beta\mathrm{COS}\theta \tag{8}$$

respectively. In Equation 7, F_x is the chordwise variation of fin thickness, α is the angle of attack, and β is the angle of yaw. In Equation 8, R_x is the axial variation of body radius. These expressions were derived to be consistent with the small disturbance approximation. In addition, the store geometry was assumed to be a body of revolution.

The MSD equation is now represented by a suitable finite difference approximation on each of the three meshes. Due to the mixed elliptic/hyperbolic nature of transonic flow, a finite difference technique must be used that accurately represents the physics of this type of flow field. The method employed in References 4 and 5 was utilized since it approximates all aspects of a steady mixed subsonic/supersonic inviscid irrotational flow. In this approximation, domains of dependence requirements were satisfied by proper combinations of upwind and central differences. The resulting sets of difference equations were solved using a successive line over relaxation (SLOR) scheme. In the fine and crude meshes, the relaxation scheme marches along vertical lines from the upstream boundary, proceeding to the next downstream plane by working outward from the centerline to the spanwise limit of the mesh. By implementing the numerical solution in this manner, an easily invertible tridiagonal matrix was obtained for each line relaxation. However, due to the angular periodicity of the store mesh, a periodically tridiagonal matrix was obtained by implementation of the same marching scheme in the store mesh. The periodic tridiagonal solver of Steger (Reference 13) was implemented to allow rapid inversion of this matrix. This iterative scheme has proven to be a stable and reliable approach for transonic flow problems.

3.3 STORE BOUNDARY CONDITIONS

As stated previously, linearized surface boundary conditions were applied on mean surfaces consistent with the small disturbance approximation. For the store body, this mean surface, or boundary condition support surface (BCSS), was a cylinder that extended

from the upstream to downstream boundary of the store mesh. The radius of the BCSS was based on an average body radius as shown in Figure 11. Since the BCSS did not correspond to the body surface, it was necessary to modify the body surface slopes to account for the translation of the point of body boundary condition application. Boppe and Stern (Reference 8) utilized slender body theory to obtain appropriate corrections for both lifting and non-lifting cases. The correction applied to body slopes was based on equality of source strength and was given by the ratio r_B/r_{BCSS}, where r_B and r_{BCSS} are defined in Figure 11. The angle of attack correction was based on equality of doublet strength and was given by the ratio $(r_B/r_{BCSS})^2$. The corrected body boundary condition is given by

$$\phi_{r|BCSS} = \left(r_B/r_{BCSS}\right)R_x - \left(r_B/r_{BCSS}\right)^2(\alpha SIN\theta + \beta COS\theta) \qquad (9)$$

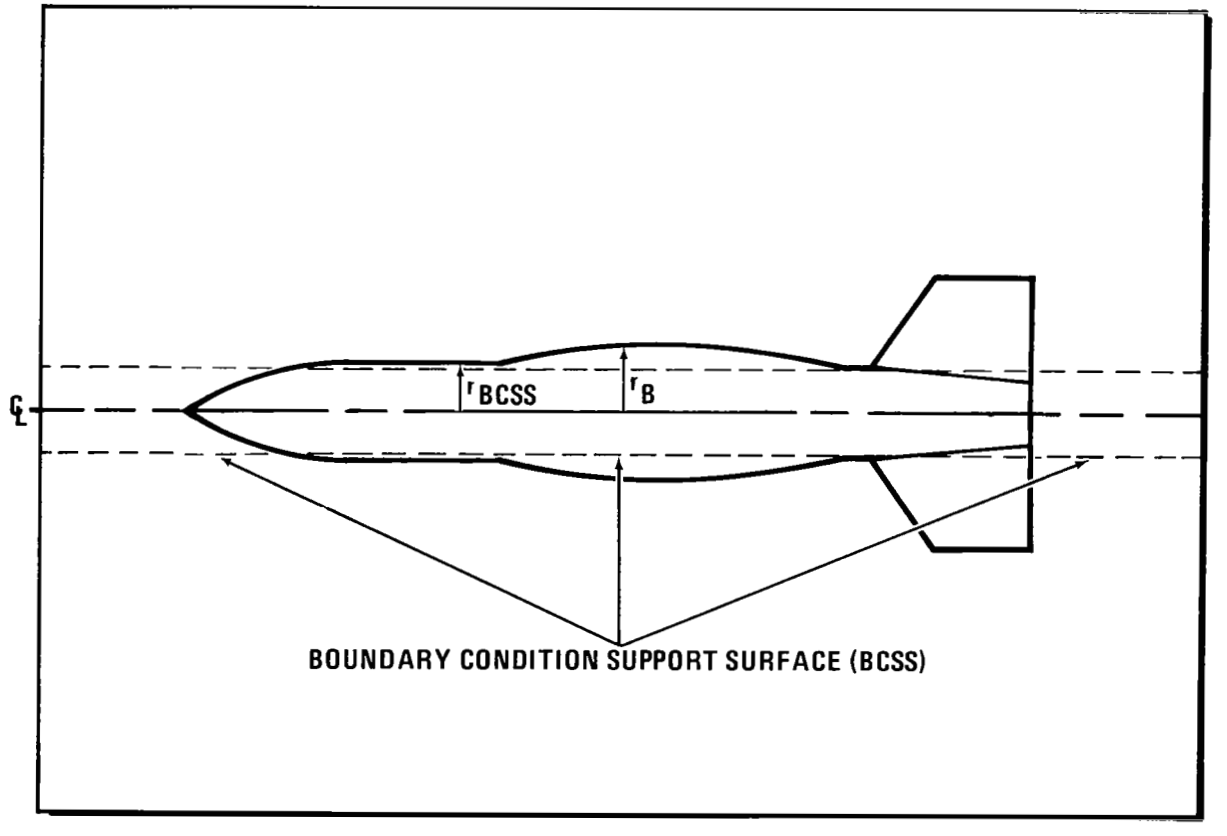

Figure 11 Store Body Boundary Conditions Were Applied On A Cylindrical BCSS

Velocities computed on the BCSS were also corrected to obtain the velocities on the true body surface. Slender body theory (Reference 8) was used to provide the necessary correction

$$\phi_{x|B} = \phi_{x|BCSS} + (r_B - r_{BCSS})[\phi_{r|BCSS}]_x \cdot \tag{10}$$

Upstream of the body, $\phi_{r\ BCSS} = 0$ was applied as the required boundary condition. Downstream of the body, Equation 9 was used with $R_x = 0$.

The body boundary condition procedure described in the preceding paragraph was found to be somewhat deficient when applied to prediction of store aerodynamics. Normal force and moment coefficients were significantly underpredicted for isolated store configurations (Reference 9). An intensive two-year study was performed under funding from the General Dynamics Internal Research and Development Program to determine the cause of this problem . The discrepancies between predicted and experimental force and moment coefficients were especially anomalous considering the apparent excellent agreement between predicted and experimental pressures (see Figures 1 and 2).

Investigation of the Nielsen generic store experimental data (Reference 10) yielded these two conclusions: (1) essentially all of the normal force and pitching moment were generated in the region near the nose, and (2) the forces and moments were generated by relatively small pressure differentials. Unfortunately, the nose region was also the location of maximum deviation of the BCSS from the body surface. Body pressures in this region were strongly influenced if not determined by the correction given in Equation 10. Accuracy of predicted forces and moments was strongly coupled to the body pressure extrapolation technique. Since the magnitude of store forces and moments was small, predictions were overly sensitive to inaccuracies of the method. Several theory modifications were implemented with no significant improvement (Reference 9). An empirical correction was developed during the IRAD study based on comparisons with the TAXI (Reference 14) and PAN AIR (Reference 15) codes for nonlifting and lifting bodies. The body pressure extrapolation (Equation 10) with the empirical correction is given by

$$\phi_{x|B} = \phi_{x|BCSS} + \mu(x)(r_B - r_{BCSS})[\phi_{r|BCSS}]_x + \nu(\theta,x) \tag{11}$$

where $\mu(x)$ is a nonlifting empirical correction given by

$$\mu(x) = (1-|\,SIN(R_x)\,|)M_\infty^{1/2} \tag{12}$$

and $\nu(\theta,x)$ is a lifting empirical correction given by

$$\nu(\theta,x) = 2/3\ M_\infty^{1/2}\ |SIN(R_x)|\ ((1+SIN\theta)\alpha+(1+COS\theta)\beta) \tag{13}$$

As reported previously, including the empirical correction significantly improved force and moment predictions. This correction was also implemented in the TAS code.

Fin boundary conditions were satisfied on planes of constant θ. Unlike the body boundary conditions, fin boundary conditions were not modified to account for the distance between the actual fin surface and the fin mean plane. The fin Kutta condition was satisfied by introducing a vortex sheet from the trailing edge of each fin to the downstream boundary of the computational domain. Across each vortex sheet, ϕ was discontinuous due to a jump in potential that was introduced to account for fin lift. ϕ_x and ϕ_r were continuous across the vortex sheet. The TAS code was developed with the capability to simulate a store without fins or with four cruciform fins with arbitrary angular displacement. The code can easily be modified to simulate up to four fins with arbitrary angular orientation.

3.4 MESH INTERFACE BOUNDARY CONDITIONS

As described in Section 3.1, boundary conditions applied at the outer boundary of the store mesh and at the SFFSS were defined by interpolation from the appropriate surrounding mesh. The interpolations employed to transfer the boundary conditins are now discussed. Boundary conditions applied at the outer boundary of the store mesh were transferred from the fine and crude meshes by either linear or natural cubic spline interpolation. Boundary conditions applied at the SFFSS were transferred from the store mesh by linear interpolation only. Both the linear and cubic spline methods were implemented as a series of one-dimensional operations to achieve the desired three-dimensional interpolation. To illustrate this procedure, consider linear interpolation of from mesh A to a point (z_B, y_B, x_B) on mesh B. Assume, for simplicity, that mesh A is a Cartesian mesh. The geometry of mesh B is not relevant. First, the eight mesh A points surrounding (z_B, y_B, x_B) must be determined. Figure 12 illustrates the nomenclature used

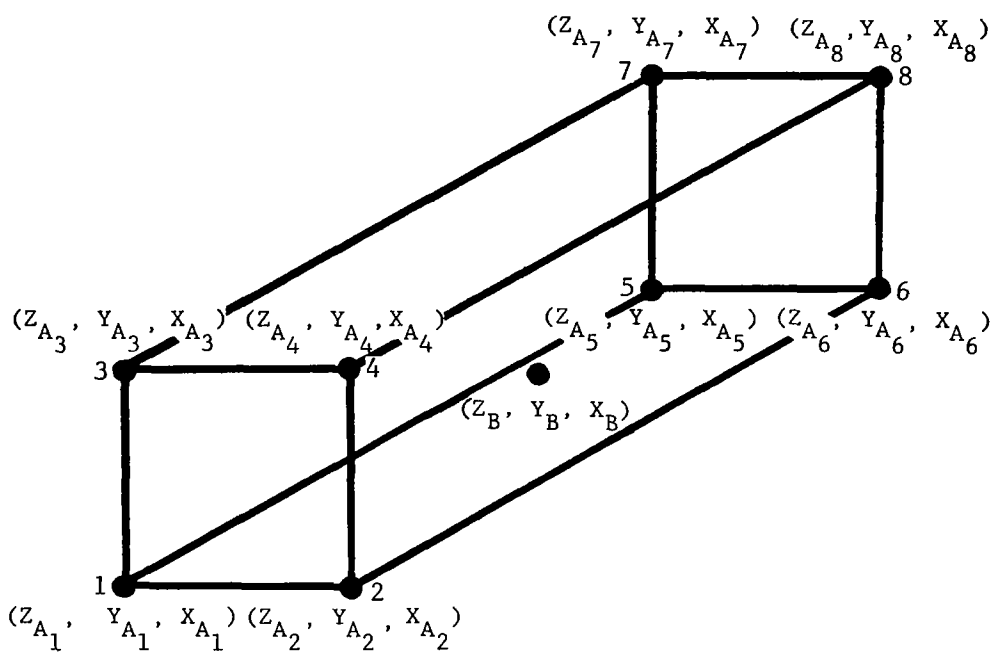

Figure 12 Points 1-8 In Mesh A Were Required To Interpolate ϕ To The Point In Mesh B

for this example. First, four one-dimensional interpolations in the x direction are performed

$$\begin{aligned} F_1 &= \phi_1 + (\phi_5 - \phi_1)\delta x/\Delta x \\ F_2 &= \phi_2 + (\phi_6 - \phi_2)\delta x/\Delta x \\ F_3 &= \phi_3 + (\phi_7 - \phi_3)\delta x/\Delta x \\ F_4 &= \phi_4 + (\phi_8 - \phi_4)\delta x/\Delta x \end{aligned} \tag{14.a}$$

where $\delta X = X_B - X_{A_1}$ and $\Delta X = X_{A_5} - X_{A_1}$.

Then two one-dimensional interpolations are performed in the y direction

$$\begin{aligned} F_5 &= F_1 + (F_2 - F_1)\delta y/\Delta y \\ F_6 &= F_3 + (F_4 - F_3)\delta y/\Delta y \end{aligned} \tag{14.b}$$

where $\delta Y = Y_B - Y_{A_1}$ and $\Delta Y = Y_{A_2} - Y_{A_1}$.

After the operation defined by (14.b) is performed, a single interpolation in the z direction is required to obtain ϕ_B

$$\phi_B = F_5 + (F_6 - F_5)\delta z/\Delta z \tag{14.c}$$

where $\delta Z = Z_B - Z_{A_1}$ and $\Delta Z = Z_{A_3} - Z_{A_1}$.

Note that no attempt is made to insure that correct domain of dependence requirements are enforced. The cubic spline interpolation is implemented in an identical manner except that sixty-four points are required to perform the interpolation instead of eight. A natural cubic spline was selected to perform the interpolation because this particular spline technique minimizes the oscillatory nature of the approximation. The higher-order interpolation was implemented only on the store mesh outer boundary because the fine and crude mesh discretizations were significantly coarser than the store mesh discretization. When interpolating from the store mesh to the fine or crude mesh SFFSS, linear interpolation was sufficiently accurate due to the finer, relative to the fine and crude meshes, discretization employed in the store mesh.

Dirichlet (potential) boundary conditions were implemented directly in the manner described in the preceding paragraph. Linear or natural cubic spline interpolations were used to interpolate boundary conditions applied on the store mesh outer boundary. Implementation of Dirichlet boundary conditions was relatively straightforward and did not require significant modification of the fine and crude mesh solution algorithms.

The capability to apply Neumann (velocity) boundary conditions on the store mesh outer boundary and SFFSS was also developed. Implementation of Neumann boundary conditions was more complex since the solution algorithm on each mesh was altered significantly. In addition, the velocities that were used to define the interpolated boundary condition also had to be computed. The velocity boundary condition interpolation was the linear interpolation defined by Equations 14.a, 14.b, and 14.c. Due to increased complexity, the cubic spline interpolation was not implemented. Implementation of the Neumann boundary condition in the finite difference approximation required interpolation of the velocities to mesh half-cell points as opposed to the actual mesh points. All velocities were computed by second-order central differences of the perturbation potential. The velocities were transformed to the appropriate boundary condition using Equations 3 or 4.

There were two regions of the SFFSS that required special treatment: (1) the front face within the store BCSS and (2) the portion of the SFFSS that extended downstream of the store mesh. It was possible for fine or crude mesh points on the front face of the SFFSS to be located within the BCSS of the store mesh where no calculations were performed. This problem was alleviated by implementing a procedure at the front face of the SFFSS that linearly interpolated from the points exterior to the BCSS to those located inside the BCSS. Boundary conditions were required on the portion of the SFFSS which extended downstream of the store mesh. This extension was required to prevent the fin wakes from intersecting the fine or crude mesh since there was a discontinuity in potential across the wake. For lack of a more accurate approach a $\phi_x = 0$ or $\phi_{nx} = 0$ boundary condition was imposed on this portion of the SFFSS.

4 TAS CODE EVALUATION

Results predicted by the TAS code were evaluated by comparison with existing experimental data. Since problems with isolated store force and moment predictions had previously been encountered, experimental pressure data was desired for the evaluation. Obtaining experimental pressure data for a configuration of this type proved to be a difficult task. The configuration of Reference 10 was selected as the test case primarily because of availability. The Nielsen generic wing/body/pylon/store configuration is shown in Figure 13. The store geometry was a tangent ogive cylinder with a two caliber nose and a fineness ratio of 8.5. The wing had a four percent thick symmetric section and an idealized F-16 wing planform. The fuselage had a circular cross section with a three caliber parabolic arc nose profile followed by a circular cylinder of constant diameter. Although the TAS code has the capability to simulate fins, this capability was not directly evaluated since the store of Reference 10 has no fins. Results presented in Section 2 show that the code adequately simulates complex fin geometries. There were two major drawbacks associated with using the data set of Reference 10 to evaluate TAS code results: (1) no experimental wing pressure distributions were obtained and (2) this configuration cannot accurately be modeled since the TAS code does not have pylon simulation capability. Therefore, the evaluation of predicted results was necessarily qualitative in some instances.

All computations reported herein were performed on the NASA ARC ACF Cray-1S. Except where noted, the pressures presented were obtained after 600 global iterations. The embedded meshes employed for these cases consisted of 117,351 mesh points (fine mesh (63 x 30 x 20), store mesh (89 x 23 x 33), and crude mesh (30 x 20 x 20)). Each global iteration of the TAS code typically required approximately 2.8 seconds. The timing was very much a function of the mesh interface boundary condition procedure. Code run times were increased by employing Neumann type boundary conditions at the mesh interfaces or by the natural cubic spline interpolation. It is important to note that the TAS code is not currently vectorized. Vectorization will probably decrease code run times by about a factor of two to three.

The baseline case that was used to study the convergence characteristics of the TAS code and evaluate the mesh interface boundary condition procedures was the configuration of Figure 13 with the store nose located 1.75 D below the wing, 4.7 D out

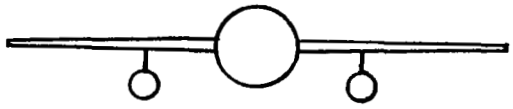

FRONT VIEW

SIDE VIEW

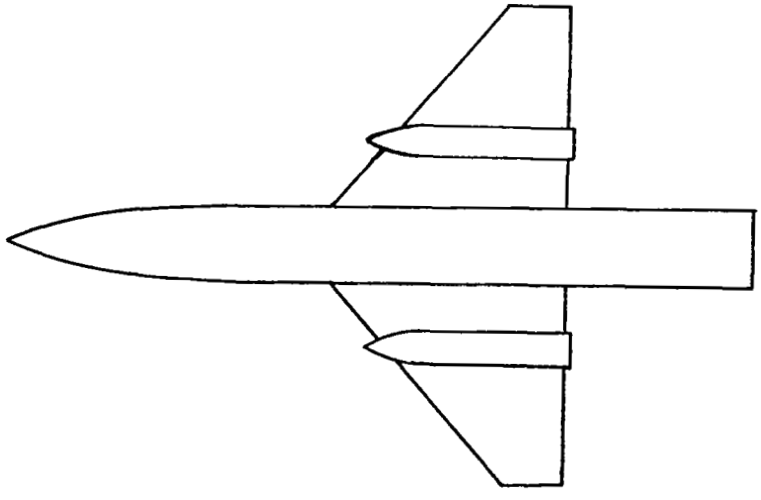

BOTTOM VIEW

Figure 13 **The Nielsen Generic Wing/Body/Pylon/Store Was Chosen To Be The Test Configuration**

the span, and 0.5 D ahead of the wing leading edge, where D is the maximum store diameter. This location corresponds to Position 1 of Configuration 13 as defined in Reference 10. Note that no attempt was made to simulate the pylon. The flight conditions were zero angle of attack and a freestream Mach number of 0.926. The fine and crude mesh SFFSS were coincident and both had a square cross section with sides approximately of length 1.85 D. The store was located in the geometric center of the SFFSS cross section. There were five spanwise and four vertical fine mesh cells on the SFFSS. The crude mesh SFFSS had three spanwise and two vertical cells. The store mesh outer boundary had a diameter of approximately three store diameters. This mesh arrangement was generated interactively in a process separate from the TAS code such that the mesh overlap requirements outlined in Section 3.1 were satisfied. Whenever these requirements were not satisfied, it was not possible to obtain a converged solution. Dirichlet boundary conditions were imposed at the mesh interfaces and linear interpolation was employed to transfer the boundary conditions between the meshes.

The convergence characteristics of the code were determined by making a series of runs of 100, 200, and 600 iterations for the configuration and flight conditions described above. The solution was behaving very well based on reduction of maximum residual until iteration 150. At this point, a short period small amplitude oscillation developed in the maximum residual in each of the meshes. This behavior continued through 600 iterations with the mean value of the oscillation slowly increasing. However, the average residual continued to decrease during this time. This seems to indicate that the oscillation in the maximum residual is a localized phenomenon that does not significantly affect the global flow field. The store and wing pressure distributions shown in Figures 14 and 15 respectively tend to support this conclusion. In both cases, the pressures are essentially unchanged from iteration 200 to iteration 600. For most engineering applications, this would be deemed a converged solution. These same convergence characteristics were observed for all cases reported here.

The computed store pressures are compared with the experimental data of Reference 10 in Figures 16 and 17 for $\theta = 85°$ and $\theta = 275°$ respectively. In both cases, but especially at $\theta = 85°$, the agreement between predicted pressures and experimental data was unacceptable in the region $0.25 \leq X/L \leq 0.75$. The flow was underaccelerated in this region since the pylon was not modeled in this simulation.

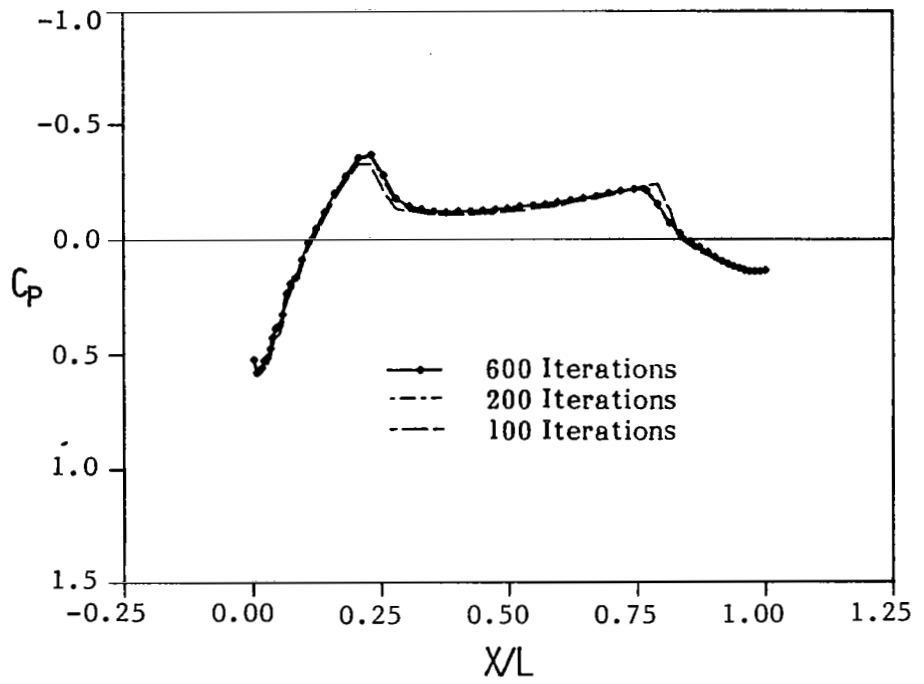

Figure 14 Store Pressures Are Essentially Unchanged After 200 Iterations

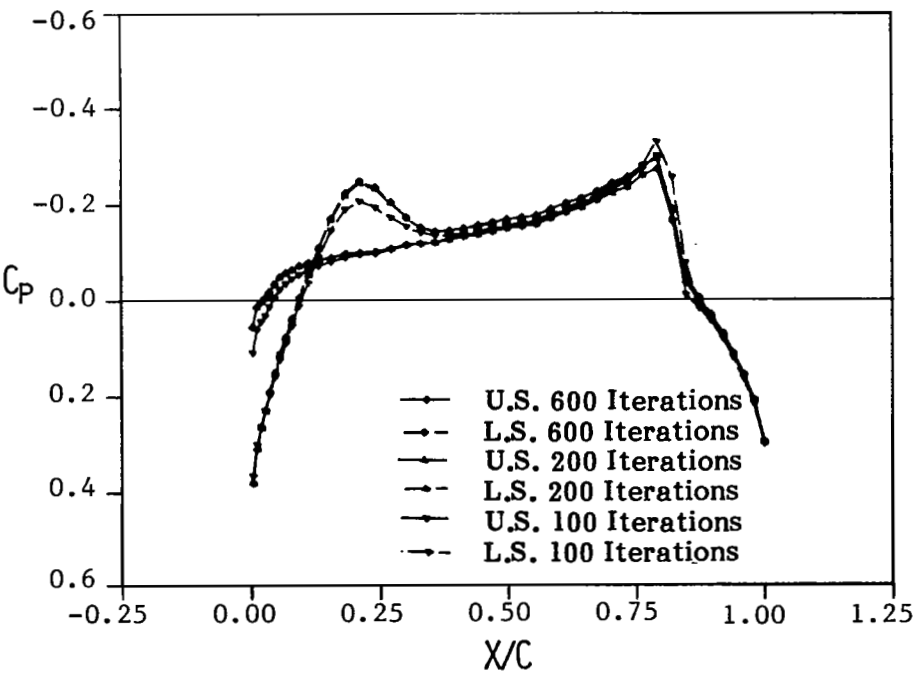

Figure 15 Wing Pressures Are Essentially Unchanged After 200 Iterations

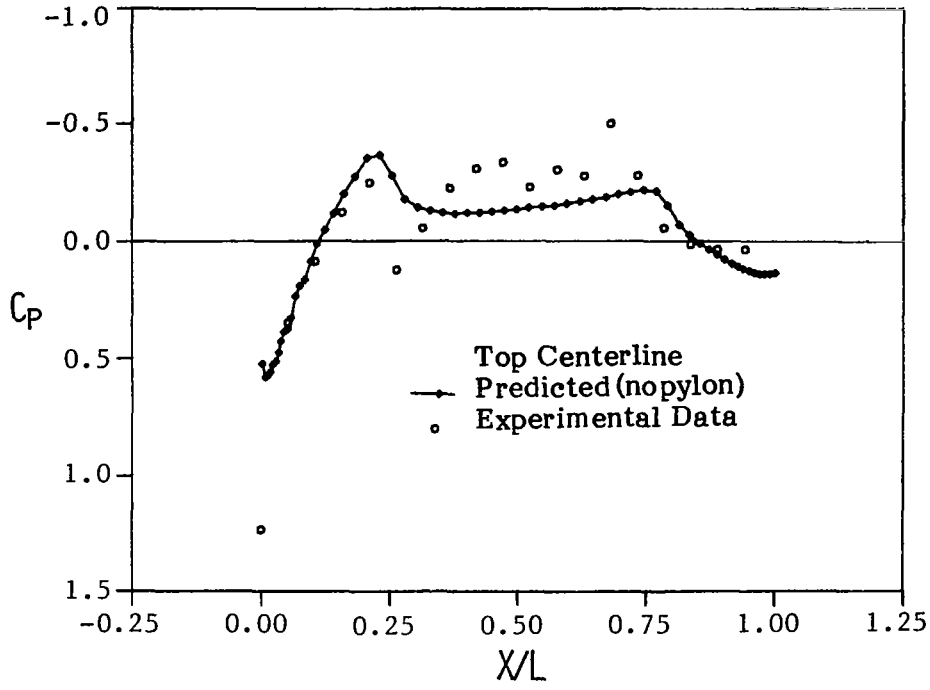

Figure 16 **Agreement Between TAS Code Predictions and Experimental Data Was Unacceptable at θ=85°**

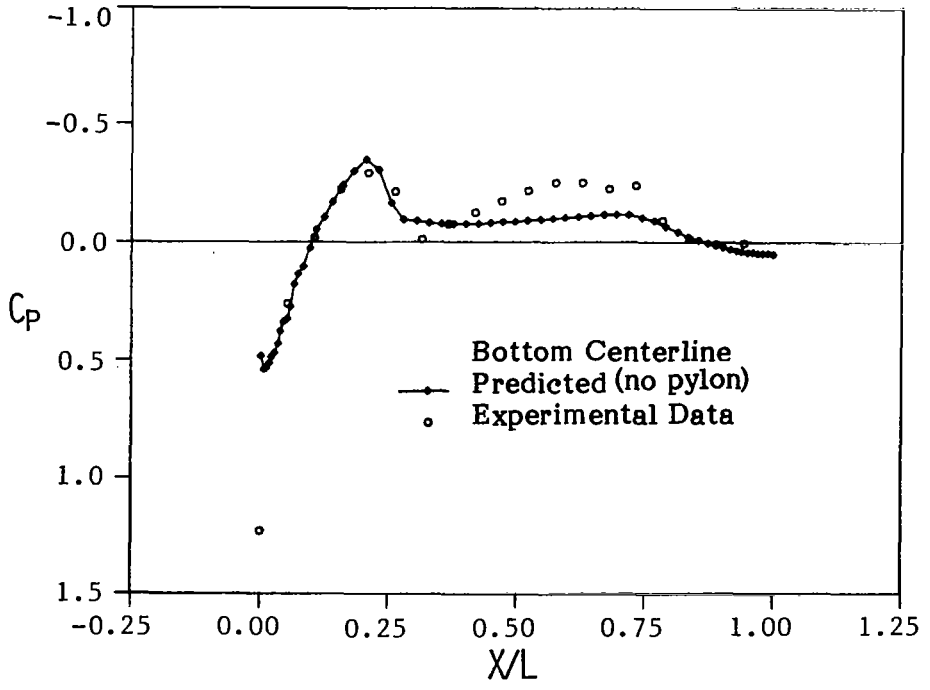

Figure 17 **Agreement Between TAS Code Predictions and Experimental Data Was Unacceptable at θ=275°**

In an attempt to improve agreement between predicted pressures and experimental data, the pylon was simulated as a single fin located at $\theta = 90°$. This was not, however, an accurate pylon simulation since no provision was made to apply pylon boundary conditions at the appropriate location in the fine and crude meshes. If the pylon could be contained completely within the SFFSS, the simulation would be adequate and acceptable. This would require the store mesh outer boundary to intersect the wing. In the current version of the TAS code, the store mesh outer boundary may not intersect or "penetrate" the wing. The effects of the pylon were indirectly transmitted to the wing through the SFFSS. Thus, correct blockage of the spanwise flow was not expected. To achieve a more accurate simulation, the span (aspect ratio) of the pylon was maintained by allowing the fin to protrude through the SFFSS and extend to the outer boundary of the store mesh violating the primary assumption concerning the SFFSS (recall that the SFFSS, as defined in Section 3.1, completely enclosed the store geometry and the associated system of fin vortex sheets). However, convergence of the iteration was not significantly affected by violating this assumption. Comparisons between predicted pressures for the store/fin and experimental data are shown in Figure 18 ($\theta = 85°$) and Figure 19 ($\theta = 275°$). Also shown in these figures are the pressures predicted for the store with no fin. From the figures, it is obvious that the fin has a significant effect on the flow field. Agreement between predicted pressures and experimental data was considerably enhanced by including the fin, especially at $\theta = 85°$. However, there was only a modest improvement in predicted store pressures at $\theta = 275°$.

A comparison between predicted force and moment coefficients and experimental data is shown in Table 1. As in the case of the isolated store, significant discrepancies were observed. Figures 20 and 21 show comparisons between the predicted and experimental axial distributions of cross section normal force coefficient and side force coefficient respectively. The predicted axial distribution of normal force followed the experimental data trends well. However, the magnitude of the negative load on the store nose ($X/L \leq 0.3$) was underpredicted by approximately a factor of two. This discrepancy was caused by the inaccuracy of the body pressure extrapolation (see Section 3.3) for $X/L \leq 0.20$ and the forward-shifted shock location on the bottom centerline at $X/L \approx 0.25$ (see Figure 19). The same shock location behavior has been observed (Reference 15) for the isolated store code and the TAXI code. In both cases, the experimental data showed the shock to be located aft of the location predicted by the conservatively differenced numerical solution. This was contrary to typical conservatively differenced wing solutions where the predicted shock location was aft of the location shown by experimental data.

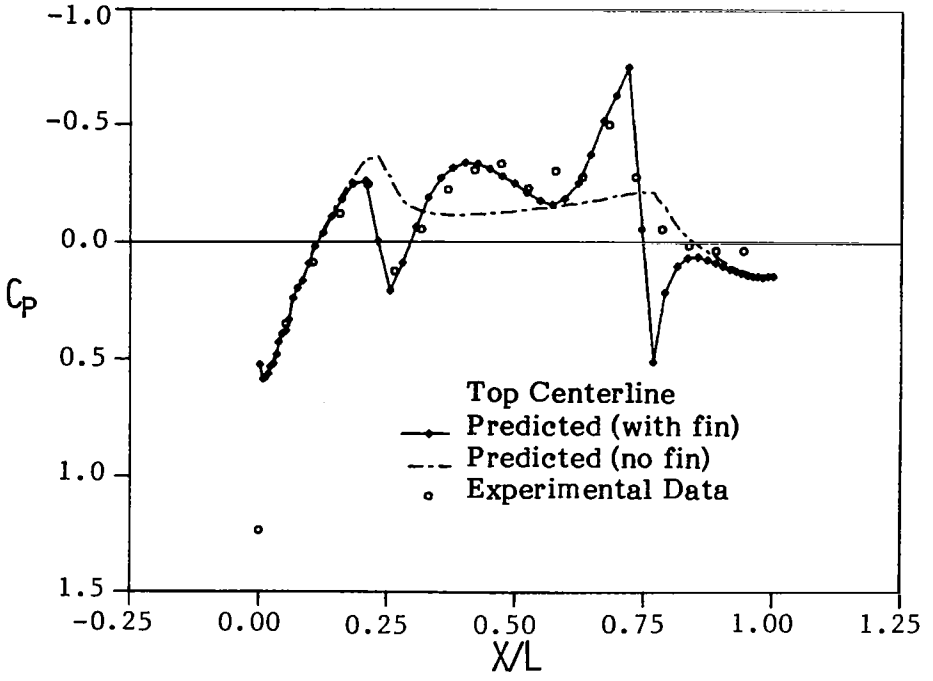

Figure 18 Simulating The Pylon As A Fin Significantly Improves Agreement With Experimental Data At θ=85°

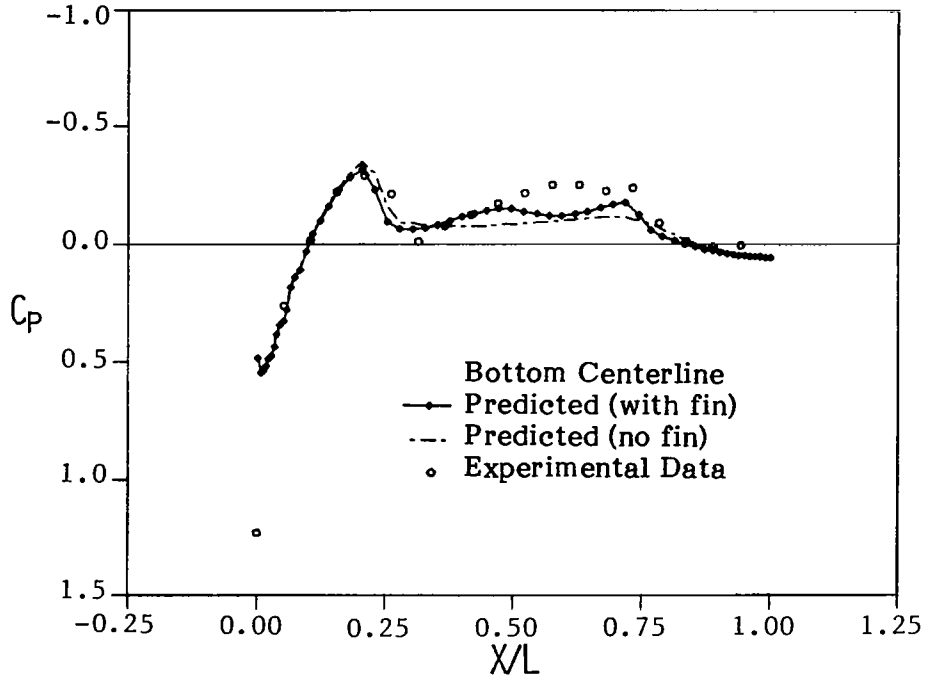

Figure 19 Simulating The Pylon As A Fin Significantly Improves Agreement With Experimental Data At θ=275°

$M_\infty = 0.926 \quad \alpha_W = \alpha_S = 0°$

	Predictions	Exp. Data
C_N	0.244	0.152
C_S	-0.105	-0.108
C_A	0.050	0.086
C_{NM}	-0.012	-0.607
C_{SM}	-0.349	-0.066

TABLE 1 SIGNIFICANT DISCREPANCIES WERE OBSERVED BETWEEN PREDICTED FORCE AND MOMENT COEFFICIENTS AND TEST DATA

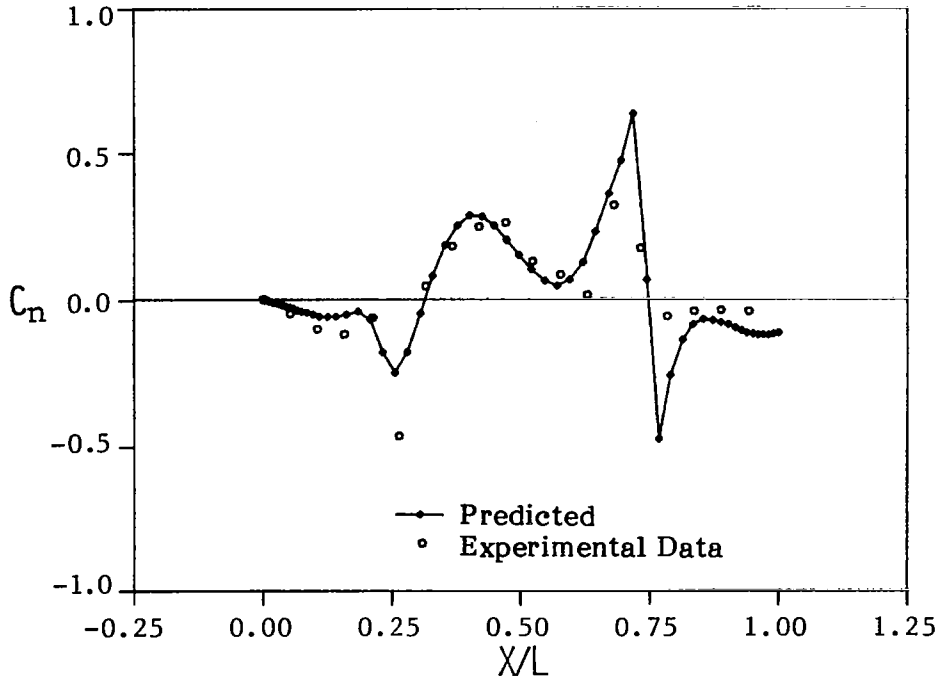

Figure 20 **Predicted Axial Distribution of C_n Shows Good Agreement With Experimental Data**

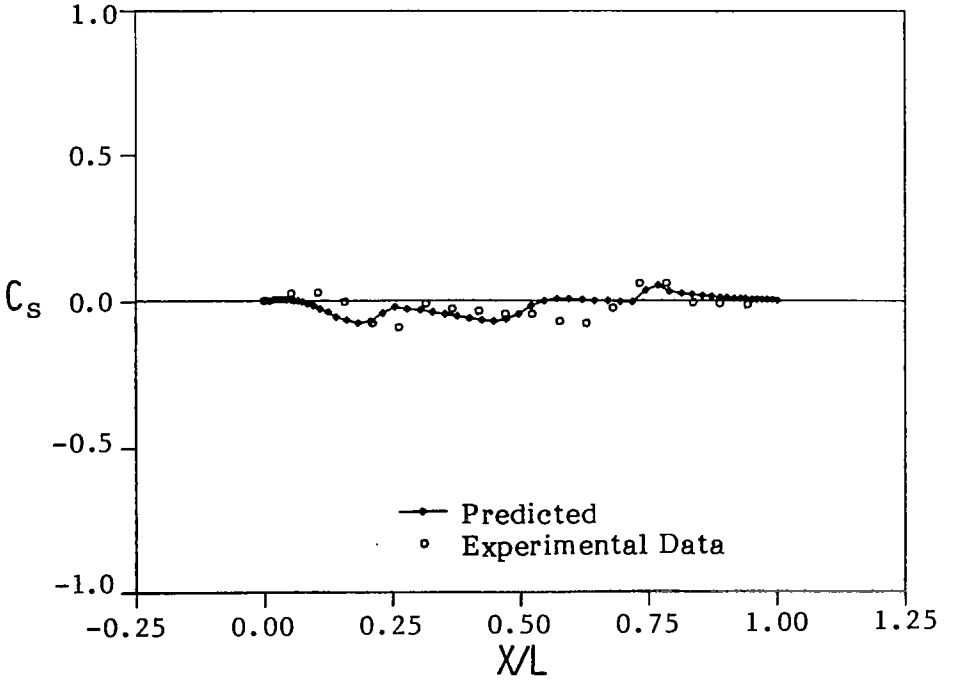

Figure 21 **Predicted Axial Distribution of C_s Shows Only Fair Agreement With Experimental Data**

There were also discrepancies in the axial distribution of C_n aft of X/L = 0.75 that were caused by an unrealistically strong shock. Results in this region could be improved by adding a viscous correction. The combination of these two discrepancies caused the error in C_N prediction. Since C_n was not accurately predicted at large moment arms (X_{MO}/L = 0.5), the corresponding moment, C_{NM}, was inaccurately predicted. As Figure 21 and the discrepancy in C_{SM} indicate, the agreement between the predicted and experimental values of C_S was merely fortuitous. These discrepancies were attributed to the incomplete pylon simulation since the blockage of spanwise flow by the pylon could not be simulated.

Figure 22 shows the predicted wing section pressure distributions for the wing/body/fin/store at the span station where the store is located. As stated previously, no wing pressures were obtained experimentally, so a qualitative comparison is made with predicted wing/body (no store) pressures at the same span station. The wing upper surface pressures were only slightly affected by the presence of the store and fin. The wing lower surface pressures were accelerated and decelerated in a manner consistent with the observed store pressure distribution and a negative lift was produced at this section. These results were intuitively correct. In Figure 23, a pseudo-three-dimensional plot of wing surface pressures is displayed. Inboard and outboard of the store, the influence of the store was attenuated in a believable manner. Since the pylon was not simulated, the correct spanwise variations in pressure may not be shown by these data. In the region of the span near the store, the store effect was largest and the shock was strengthened and shifted forward.

The effect of mesh interface boundary condition type was investigated by applying Neumann boundary conditions (as described in Section 3.4) at the mesh interfaces. The two boundary condition types, Dirichlet and Neumann, transmitted different types of information between the flow fields. The Dirichlet boundary conditions imposed the perturbation velocity potential. In essence, the velocity distribution tangential to the boundary was specified. The Neumann boundary conditions imposed the velocity distribution normal to the surface. At the outset it was not evident that one was preferable to the other, except that the Neumann boundary condition would require more computer time. Figure 24 and Figure 25 show a comparison between store pressures predicted using Neumann and Dirichlet boundary conditions at the mesh interfaces and experimental data at $\theta = 85°$ and $\theta = 275°$ respectively. In both instances, the pressures predicted employing Neumann boundary conditions were displaced downward in the region

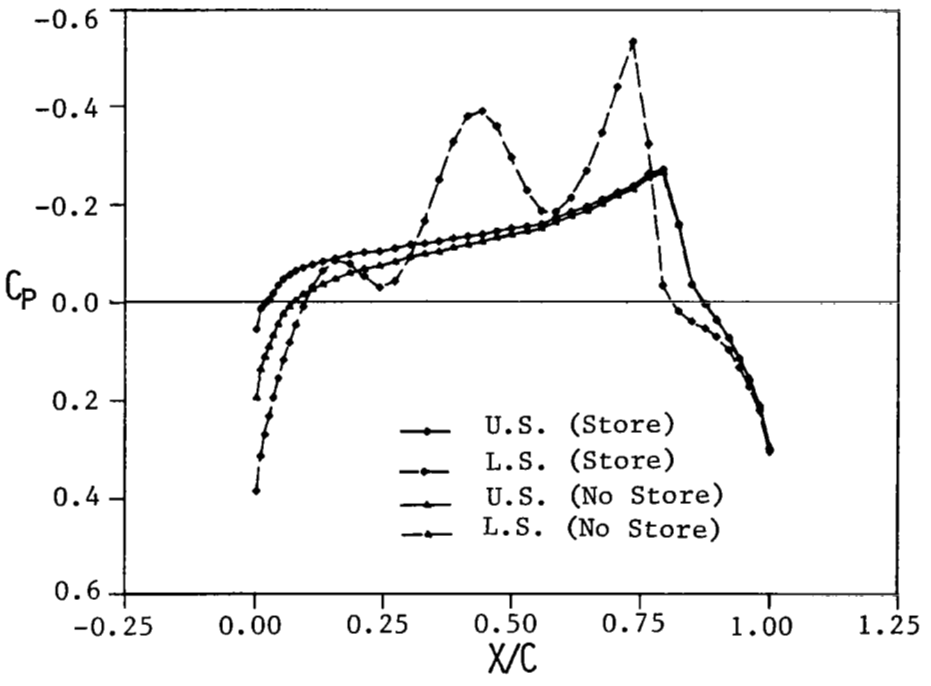

Figure 22 Predicted Wing Pressures Show the Expected Trends

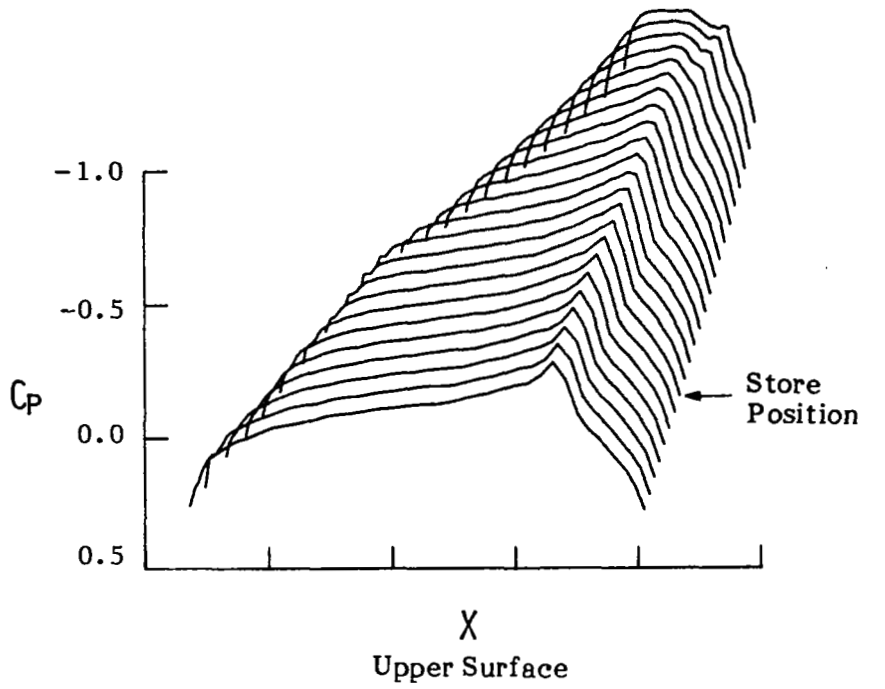

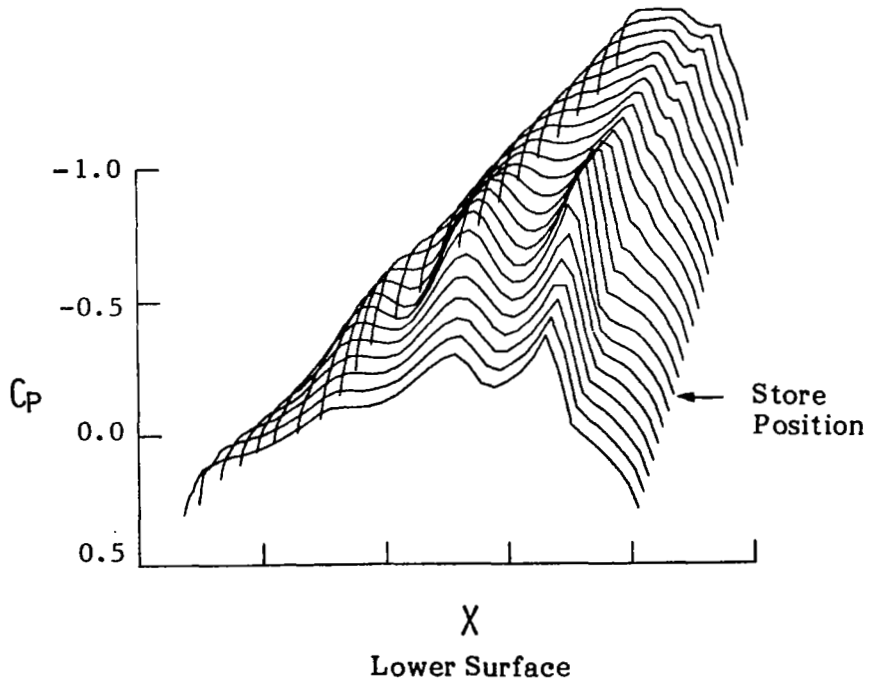

Figure 23 Influence of Store On Wing Surface Pressures Appears Reasonable

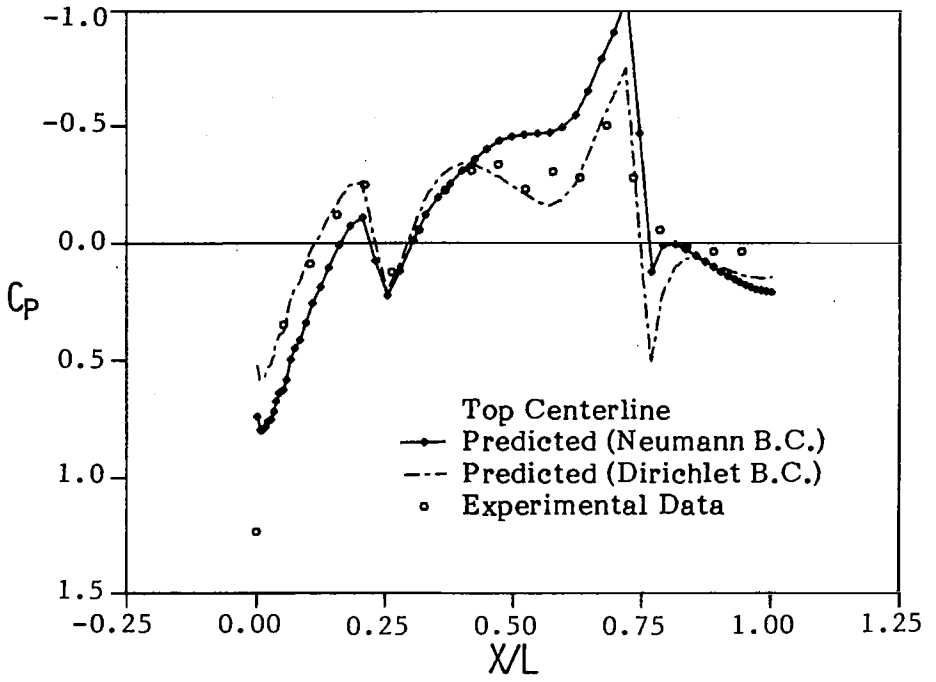

Figure 24 Neumann Boundary Conditions Produce Different Results At θ=85°

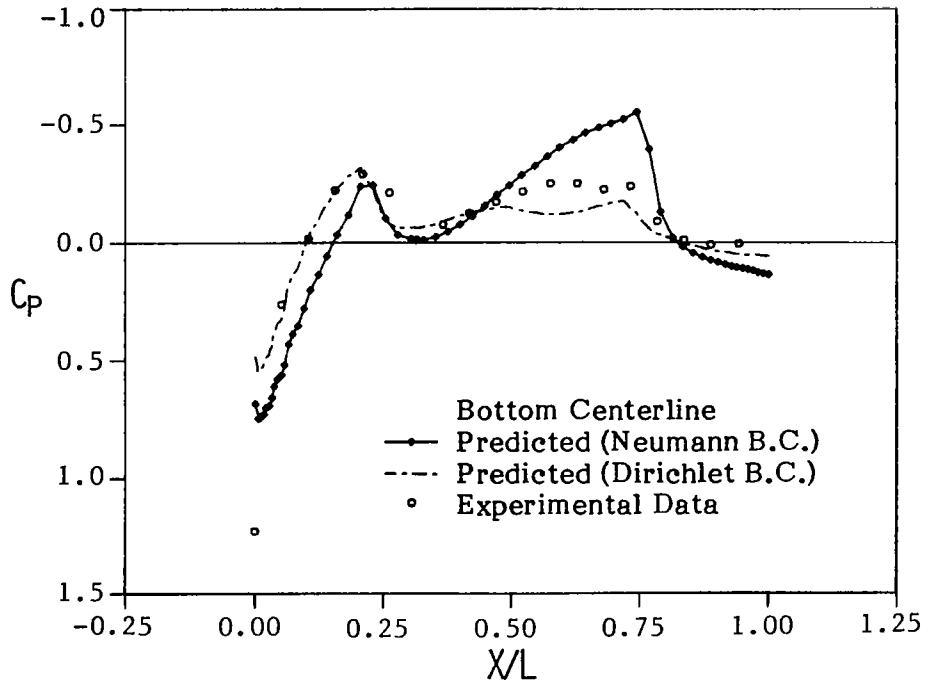

Figure 25 Neumann Boundary Conditions Produce Different Results At θ=275°

$0.05 \leq X/L \leq 0.25$. In the region $0.5 \leq X/L \leq 1.0$, the flow was overaccelerated and did not follow the experimental data. These effects were transmitted to the wing through the SFFSS. This solution required four percent more computer time than the Dirichlet boundary condition case. Atta and Vadyak (Reference 16) have employed grid embedding for a wing/pylon/nacelle configuration by modifying the full potential equation solution code TWING. At the time that Reference 16 was published, a mutually interacting solution had not been obtained. According to Reference 16, the "one-way" interaction solution obtained by the TWPN code was independent of the type of boundary condition applied at the mesh interfaces. The TAS code was modified to allow the wing/body and store solutions to be decoupled. "One-way" interaction solutions generated by the TAS code showed that: (1) the Neumann and Dirichlet boundary conditions implemented at the SFFSS give essentially the same solution and (2) different boundary conditions applied at the store mesh outer boundary give different results. Since the Dirichlet boundary conditions show better agreement with experimental data, the differences between results predicted using Dirichlet and Neumann boundary conditions (Figures 25 and 26) are attributed to a FORTRAN error that has not been discovered. For this reason, the Neumann boundary condition option was not evaluated further.

The natural cubic spline interpolation of Section 3.4 was implemented to investigate the effects of interpolation order on convergence and prediction accuracy. The higher-order interpolation was implemented only at the store mesh outer boundary interface for reasons explained in Section 3.4. Figures 26 and 27 show a comparison between store pressures predicted using the cubic spline and linear interpolations and experimental data for $\theta = 85°$ and $\theta = 275°$ respectively. In both cases, the only significant differences occurred at $0.5 \leq X/L \leq 0.75$. The results predicted with the cubic spline interpolation show only modest improvements for the case considered. The wing pressure distribution was essentially unaffected by a these small changes. Force and moment coefficients were similarly unchanged. The convergence of the iteration was degraded slightly and a somewhat larger supersonic region was generated (approximately 10 percent more supersonic points on the same mesh system). The computer time required for 600 iterations was increased 25 percent by employing the cubic spline interpolation. However, due to the overall improved agreement between predicted pressures and experimental data, the cubic spline was retained for the remainder of this study. Further investigation of this topic is required.

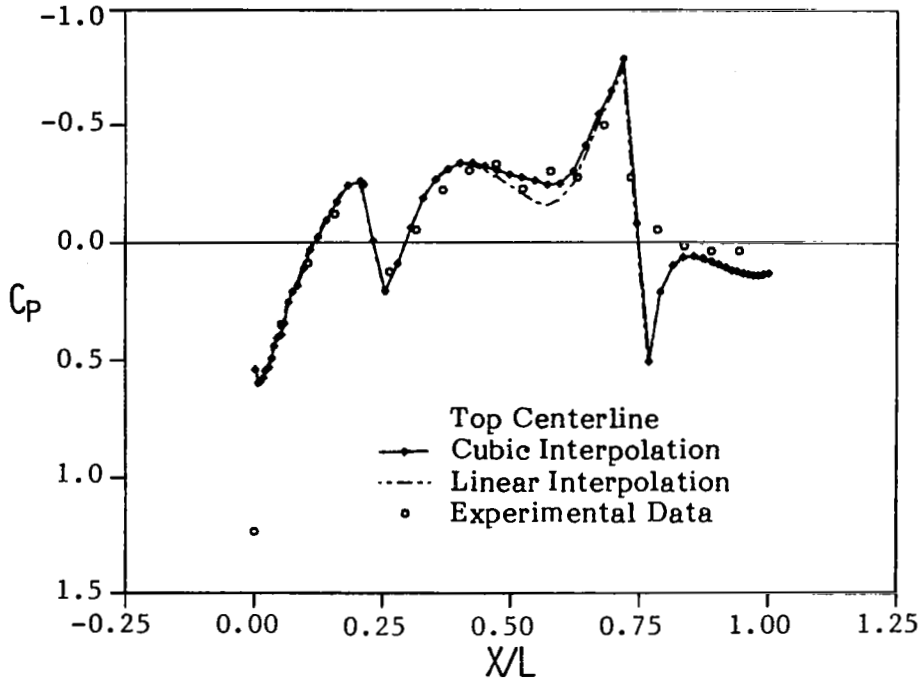

Figure 26 A Cubic Spline Interpolation Improves Predicted Pressures At θ=85°

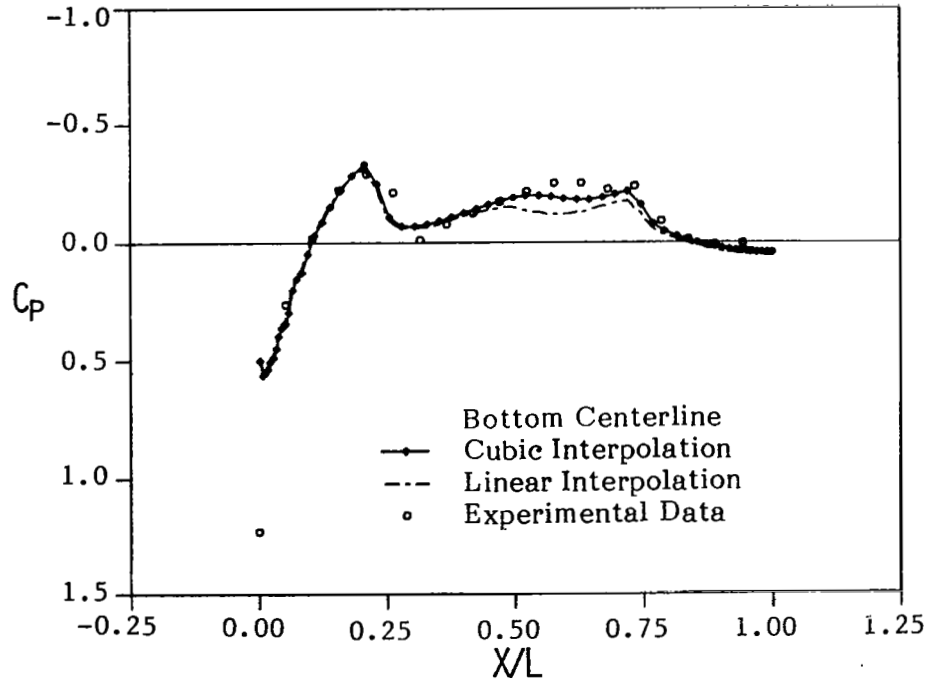

Figure 27 A Cubic Spline Interpolation Improves Predicted Pressures At θ=275°

The final step in this evaluation of the TAS code consisted of comparing predicted results for the Nielsen generic wing/body/store with the store located at three different positions: (1) 1.7 D below the wing, (2) 2.1 D below the wing, and (3) 2.5 D below the wing. The pylon could not have been simulated for Positions 2 or 3 since the present version of the TAS code does not allow simulation of a store with a separated fin. For this reason, the pylon was not simulated and no comparisons were made with experimental data. Dirichlet boundary conditions were interpolated to the mesh interfaces using the natural cubic spline interpolation. In all three cases the mesh overlap criterion were satisfied. The flight conditions were $M_\infty = 0.926$ and $\alpha_W = \alpha_S = 0°$. Figures 28 and 29 show comparisons between predicted store pressures for the three store locations at $\theta = 85°$ and $\theta = 275°$ respectively. The predicted store pressures show that the flow was accelerated and the shocks shifted aft for the store positions nearer the wing. In addition, the flow on the store nose ($X/L \leq 0.2$) was decelerated as the store was moved nearer to the wing. These effects were more pronounced at $\theta = 85°$ than $\theta = 275°$. Figure 30 shows a comparison between the predicted midspan chordwise pressures distributions on the wing for each store position. The influence of the store on the wing pressures was attenuated as the store was moved away from the wing. The pseudo-three-dimensional pressure plots of Figure 31 show this effect more clearly. The pressure peak on the lower surface increased as the store was moved nearer to the wing. In addition, the spanwise attenuation of the pressure peak is also clearly shown. The results shown in Figures 30-32 are intuitively correct. However, development of the capability to simulate a pylon will allow the code to be thoroughly evaluated by comparison with experimental data.

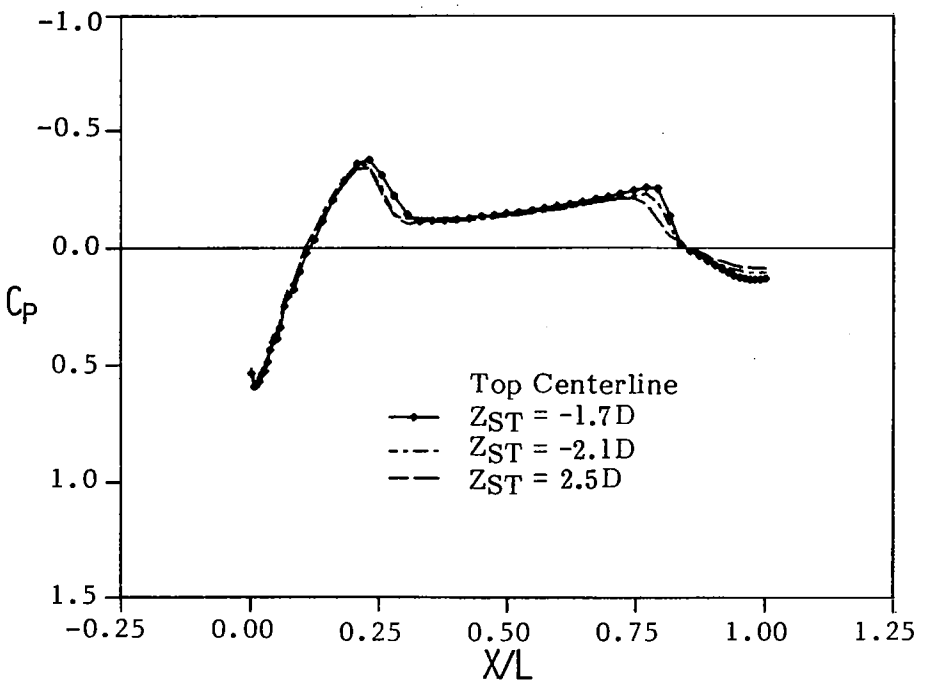

Figure 28 Predicted Store Pressures Show Effect of Store Location At θ=85°

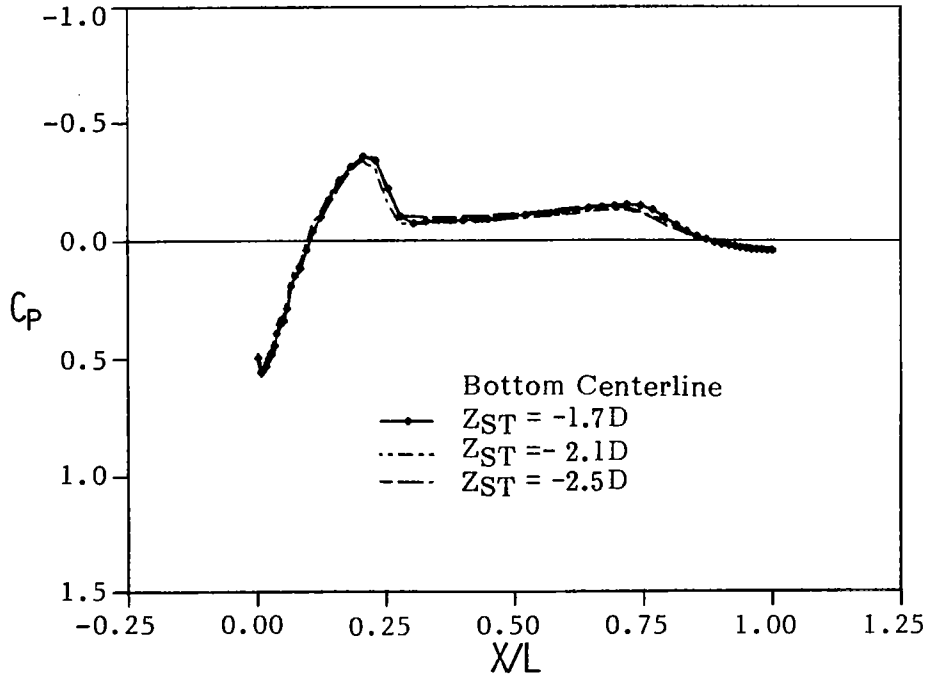

Figure 29 Predicted Store Pressures Show Effect of Store Location At θ=275°

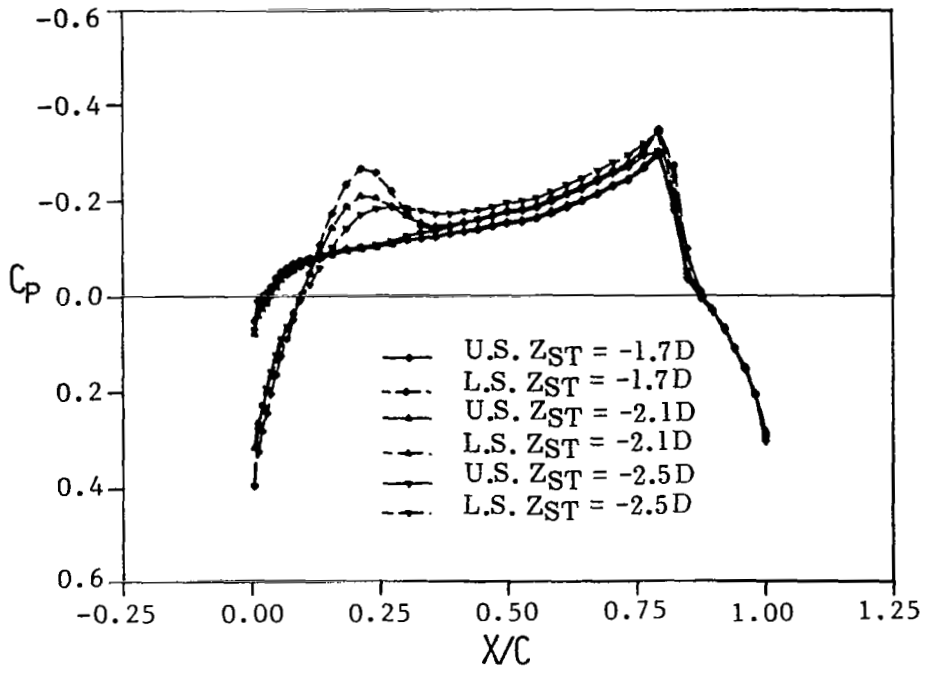

Figure 30 Midspan Wing Pressures Show Effect of Store Location

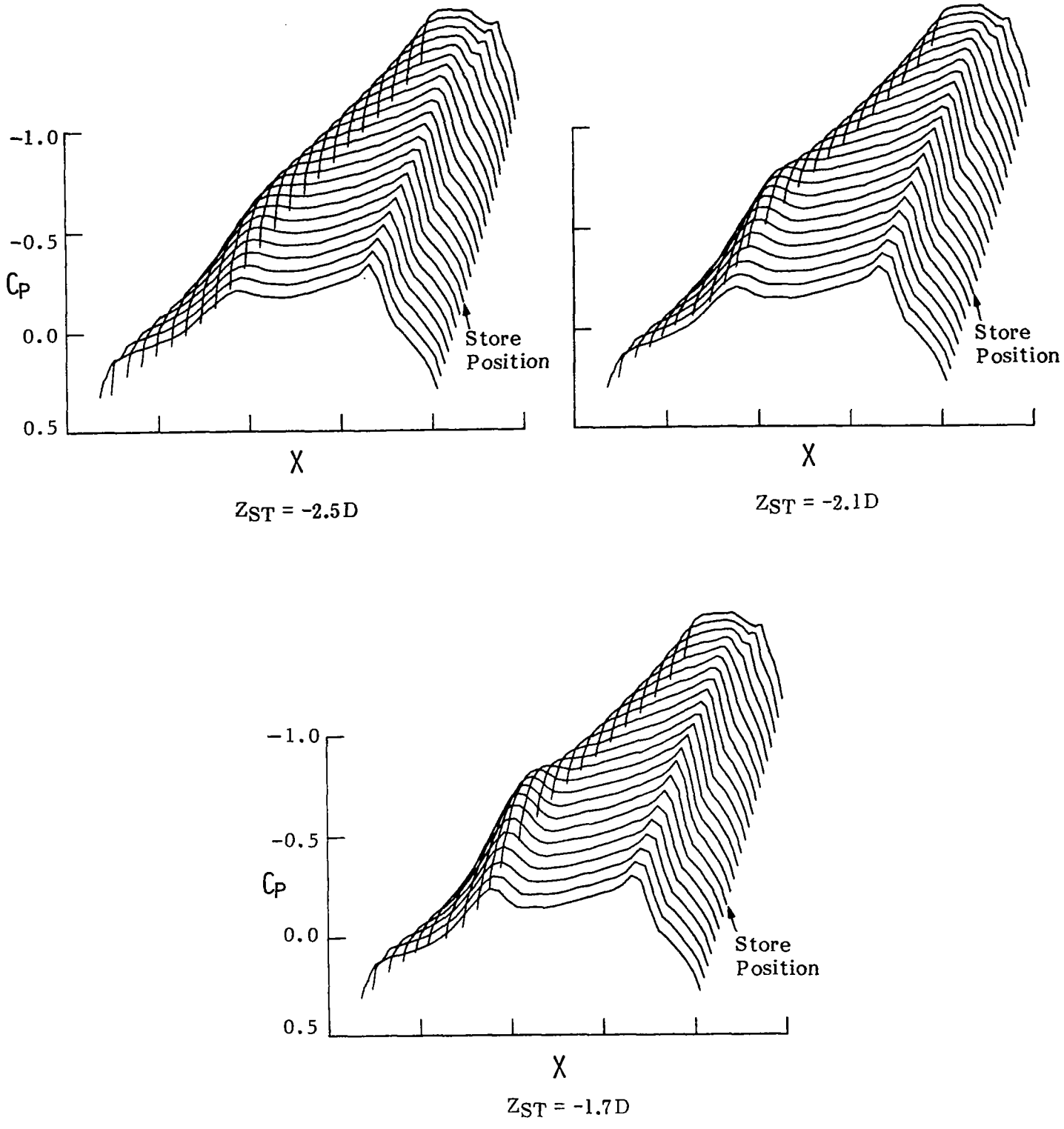

Figure 31 Wing Lower Surface Pressures Clearly Show Effect of Store Location

5 CONCLUSIONS AND RECOMMENDATIONS

A numerical method has been developed that has the capability to predict the complex flow fields associated with aircraft/store configurations in the transonic flight regime. The transonic aircraft/store flow field prediction code, TAS, can predict the transonic flow field surrounding an aircraft with an arbitrarily located, separated store. During development and validation of the code, several significant conclusions were gleaned:

1. Pressures predicted by the TAS code show good agreement with experimental data within the constraints imposed by geometry simulation. (i.e. pylon simulated as fin). Correct trends are predicted by the code for all cases considered.

2. Apparently there is an undiscovered error in the Neumann type mesh interface boundary condition procedure. This feature of the code is not essential since results computed using Dirichlet boundary conditions were determined to be acceptable. In addition, employing Neumann boundary conditions requires approximately four percent more computer time.

3. A higher-order interpolation at the mesh interfaces seems to give improved results at the cost of increased code run time. In addition, this mesh embedding approach is very sensitive with respect to mesh geometry.

4. The general concept of mesh embedding requires a rigorous analysis to determine the properties of different methods of transmitting information between the meshes.

5. Problems associated with the small disturbance formulation suggest that implementation of a more accurate formulation of the flow field governing equations should be investigated.

As with any research and development program, several areas of the code were identified as needing further development. These are:

1. The capability to simulate store carriage must be developed for the TAS code to be a useful engineering tool.

2. The TAS code should be vectorized to decrease code run times.

3. The TAS code must be made more user friendly. Features such as automatic grid generation and NAMELIST input format should be incorporated in the code.

In summary, the TAS code can analyze wing/body/store configurations and effectively discern data trends. The TAS code is a good starting point for the development of a more comprehensive numerical preocedure to predict arbitrary store loadings.

REFERENCES

1. Stahara, S.S., "Study of Transonic Flow Fields About Aircraft: Application to External Stores", AGARD CP 285, 1980.

2. Deslandes, R., "Evaluation of Aircraft Interference Effects on External Stores at Subsonic and Transonic Speeds", AGARD CP 285, 1980.

3. Shankar, V. and Malmuth, N.D., "Computational and Simplified Analytical Treatment of Transonic Wing-Fuselage-Pylon-Store Interactions", AIAA-80-0127, 1980.

4. Ballhaus, W.F., Bailey, F. R., and Frick, J., "Improved Computational Treatment of Transonic Flow About Swept Wings", NASA CP-2001, 1976.

5. Mason, W. H., MacKenzie, D. A., Stern, M. A., Ballhaus, W. F., and Frick, J., An Automated Procedure for Computing the Three-Dimensional Transonic Flow Over Wing/Body Combinations Including Viscous Effects, Volumes I-II, AFFDL-TR-77-122, 1977.

6. Meyer, R., Cenko, A., and Yaros, S., An Influence Function Method for Predicting Store Aerodynamic Characteristics During Weapon Separation, NASA TM-84729, 1981.

7. Cenko, A., Meyer, R., Tessitore, F., Dyer, R., and Lijewski, L., "Advances in Methods for Predicting Store Aerodynamic Characteristics in Proximity to an Aircraft", AIAA-83-0266, 1983.

8. Boppe, C.W., and Stern, M.A., "Simulated Transonic Flows for Aircraft With Nacelles, Pylons, and Winglets", AIAA-80-0130, 1980.

9. Thompson, D.S., "A Mesh Embedding Approach for Prediction of Transonic Wing/Body/Store Flow Fields", NASA CP-2201, 1981.

10. Stahara, S.S. and Crisalli, A.J., Data Report for a Test Program to Study Transonic Flow Fields About Wing-Body/Pylon/Store Combinations, Volumes I - III, AFOSR TR-79-1070 to 1072, 1978.

11. Shadow, T.O., Wind Tunnel Tests to Determine the Distributed Loads on A 0.25-Scale GBU-15 (CWW) Model At Transonic Mach Numbers, AEDC-TSR-80-P14, 1980.

12. Atta, E.H., "Component-Adaptive Grid Interfacing", AIAA-81-0382, 1981.

13. Steger, J.L., "Implicit Finite Difference Simulation of Flow About Aribitrary Geometries with Application to Airfoils", AIAA-77-665, 1977.

14. Holst, T.L., NASA ARC, "Personal Communication".

15. Sidwell, K.W., Baruah, P.K., and Bussoletti, S.E., PAN AIR - A Computer Program for Predicting Subsonic or Supersonic Linear Potential Flows About Arbitrary Configurations Using A Higher-Order panel Method, Volume II - Users Manual, NASA CR-3252.

16. Atta, E.H. and Vadyak, J., "A Grid Interfacing Zonal Algorithm for Three-Dimensional Transonic Flows About Aircraft Configurations", AIAA-82-1017.

APPENDIX

USE OF THE TAS CODE

The TAS Code is resident on the NASA ARC ACF Cray-1S. The source code is stored on the Cray in UPDATE format under US=STAICA/ID=STAICA as TASPL. The library utilized to execute the code, TASLIB, is stored under the same US and ID. A sample problem for the Neilsen generic wing/body/store is located on the NASA ARC VAX 11/780 network in the file JUP::DRCO:[DTHOMPSON. TAS] SAMPLE. JOB. The file contains the necessary Cray job control language to execute the TAS code. In addition, the MAIN and NAMLIST subroutines and the problem geometry are also contained in this file. The NAMLIST subroutine is employed to define the necessary input parameters. Wing, store, and fin pressure coefficients are written to TAPE30, TAPE40, and TAPE50 respectively and are saved by the sample job. Wing, store, and fin pressures can be retrieved from the Cray using the file RET. JOB. These pressures can be plotted using the programs SECCP.EXE and BODCP.EXE. In addition, the program CP3D.EXE plots a pseudo-three-dimensional wing pressure distribution. The pressure plots in Section 4 were generated using these programs.

TAS CODE INPUT

No changes have been made to the wing/body input format defined in Volume II of Reference 5. Three additional logical variables, ISTORE, NEUBCF, and NEUBCX, are defined in subroutine NAMLIST. Default refers to the value given in the sample job.

VARIABLE	DEFAULT	REMARKS
ISTORE	(T)	T - Wing/body/store solution.
		F - Wing/body solution only.

NEUBCF	(F)	T- Apply Neumann boundary conditions on fine mesh SFFSS.
		F - Apply Dirichlet boundary conditions on fine mesh SFFSS.
NEUBCX	(F)	T - Apply Neumann boundary conditions on crude mesh SFFSS.
		F - Apply Dirichlet boundary conditions on crude mesh SFFSS.

The store input data also follow the format established for the wing body in Volume II of Reference 5. It is necessary to define several additional variables that specify store flight conditions (with the exception of Mach number and gamma that are defined in the wing/body portion of subroutine NAMLIST), store input geometry format, and whether the store mesh is user generated or automatically generated by the code. These variables are defined in subroutine NAMLIST.

VARIABLE	DEFAULT	REMARKS
IFINRS	(T)	T - Read in XINS, ETAS, and ZTS Meshes.
		F - Use internally generated meshes.
IMAPRS	(F)	T - Read in Mapping of $\xi = 0$ and $\xi = 1$ lines.
		F - Use internally generated mapping.

IFOILS	(T)	T - Fin section input consists of one (X,Z) pair per card. F - Fin section input consists of blocks of X's and Y's (old Ames input format).
IBODIS	(T)	T - Simplified body input - automatic slopes. F - Input detailed body slopes (NA).
AXISYS	(T)	T - Axisymmetric body. F - Non-axisymmetric body (NA).
AREAS	(F)	T - Z body coordinates are areas. F - Z body coordinates are Z's.
FIN	(F)	T - Solution obtained for store without fins. Note: Fin gemoetry must still be specified for mesh generation.
NEUBCS	(F)	T - Apply Neumann boundary conditions on store mesh outer boudary. F - Apply Dirichlet boundary conditions on store mesh outer bounary.

OVFAC	0.15	Minimum fraction of fine/store and crude/store mesh overlaps
ALPHAS	0.0	Store angle of attack relative to the freestream velocity in degrees.
BETAS	0.0	Store angle of yaw relative to the freestream velocity in degrees.
DTH	0.0	Angular displacement of Fin #1. (Fin #1 originally located at $\theta = 0°$)
XSTO	11.967	X ordinate of store nose (XS = 0)
YSTO	3.5	Y ordinate of store nose.
ZSTO	-1.95	Z ordinate of store nose

N.A. - Not available at this stage of development.

At the current stage of TAS code development, it is suggested that the user generate the meshes used in the numerical solution. This will insure that the necessary mesh overlap criterion are satisfied. In the next phase of TAS code development, the fine, store, and crude mesh generation algorithms will be integrated to form a single mesh generation subroutine. This subroutine will automatically generate the three meshes such that they satisfy the necessary mesh overlap criterion.

1. Report No.	2. Government Accession No.	3. Recipient's Catalog No.
NASA CR-3721		

4. Title and Subtitle	5. Report Date
TAS - A TRANSONIC AIRCRAFT/STORE FLOW FIELD PREDICTION CODE	December 1983
	6. Performing Organization Code
7. Author(s)	8. Performing Organization Report No.
D. S. Thompson	
	10. Work Unit No.
	T6457
9. Performing Organization Name and Address	11. Contract or Grant No.
General Dynamics Corporation, Fort Worth Division P.O. Box 748 Fort Worth, TX 76101	NAS2-11277
	13. Type of Report and Period Covered
12. Sponsoring Agency Name and Address	Contractor Final Report July 1982 to May 1983
National Aeronautics and Space Administration Washington, DC 20546	14. Sponsoring Agency Code
	505-31-01

15 Supplementary Notes Point of Contact: Paul Kutler/M.S. 202A-14/Ames Research Center, Moffett Field, CA 94035/(415) 965-6032 or FTS 448-6032

16 Abstract

A numerical procedure has been developed that has the capability to predict the transonic flow field around an aircraft with an arbitrarily located,, separated store. The TAS code, the product of a joint General Dynamics/NASA ARC/AFWAL research and development program, will serve as the basis for a comprehensive predictive method for aircraft with arbitrary store loadings. This report describes the numerical procedures employed to simulate the flow field around a configuration of this type. The validity of TAS code predictions is established by comparison with existing experimental data. In addition, future areas of development of the code are outlined. A brief description of code utilization is also given in the Appendix.

The aircraft/store configuration is simulated using a mesh embedding approach. The computational domain is discretized by three meshes: (1) a planform-oriented wing/body fine mesh, (2) a cylindrical store mesh, and (3) a global Cartesian crude mesh. This embedded mesh scheme enables simulation of stores with fins of arbitrary angular orientation. The finite difference approximation for a modified version of the transonic small disturbance potential equation is iteratively solved on each mesh by a line relaxation algorithm. Each global iteration consists of successive fine/store/crude mesh relaxations. Boundary conditions applied at the mesh interfaces are updated during the course of each iteration.

17. Key Words (Suggested by Author(s))	18. Distribution Statement
Transonic Aircraft/Store Computational aerodynamics Mesh embedding	Unclassified - Unlimited Subject Category 02

19. Security Classif. (of this report)	20. Security Classif. (of this page)	21. No. of Pages	22. Price*
Unclassified	Unclassified	57	A04

*For sale by the National Technical Information Service, Springfield, Virginia 22161

NASA-Langley, 1983